PARTICLES PRODUCED IN ASSOCIATION WITH PSI(3098)

BY

GEORGE OSCAR ALVERSON

B.S., California Institute of Technology, 1973
M.S., University of Illinois, 1974

THESIS

Submitted in partial fulfillment of the requirements
for the degree of Doctor of Philosophy in Physics
in the Graduate College of the
University of Illinois at Urbana-Champaign, 1979

Urbana, Illinois

PARTICLES PRODUCED IN ASSOCIATION WITH PSI(3098)

George Oscar Alverson, Ph.D.
Department of Physics
University of Illinois at Urbana-Champaign, 1979

Dimuon production has been studied at 217 Gev/c in π^--hydrogen and π^--beryllium collisions with a multiparticle spectrometer to detect associated particles. Particular attention has been paid to the $\psi\gamma$ spectrum which shows an excess of events in the region 3.5 Gev. Attributing this to the presence of the $\chi(\sim 3.5)$ states implies that 94±50% of psis are produced via radiative chi decay.

ACKNOWLEDGMENTS

I would like to thank all those people who helped me to complete this thesis work. In particular I would like to thank my advisor, Lee Holloway, and my co-workers on Fermilab Experiment E369. I would also like to mention those people who aided me with personal support-- John and Sandy Cooper, Mike Shupe, Bill Francis, and Waldo MacKay--while working on E369, and those who helped me throughout my graduate career--Kevin Schmidt, Chris Shea, and Alan Bross.

This thesis is dedicated to my loving parents.

The work presented in this thesis was supported in part by the U.S. Department of Energy under grant EY-76-C-02-1195.

TABLE OF CONTENTS

CHAPTER 1.

INTRODUCTION

In November of 1974 an event occurred which echoed many previous events in physics--the discovery of an almost completely unexpected phenomenon. In this case it was simultaneously revealed by experimental groups on the East and West Coasts [1,2] that they had found a new exceedingly massive and exceedingly long-lived particle (3.097 Gev and width = 67 Kev by the latest data[3]),and had named it the J or psi respectively.

At that time, experimental high energy physics, especially that part dealing with the strong interactions , was in the doldrums, the last exciting event being the discovery of weak neutral currents at Gargamelle in 1973[4], and before that , CP violation in 1964. The prediction of the existence of weak neutral currents was a primary feature of the model of Weinberg and Salam which was a renormalizable, non-Abelian group theory uniting the weak and the electromagnetic interactions. While experimentalists worked at refining their measurements of parameters which could be predicted by a Weinberg-Salam type model, theorists were busy building models

combining Weinberg-Salam and the strong interaction. It was mainly to remove some difficulties with these combined theories that a new additive quantum number called charm gained favor [5], even though the idea was originally proposed by Bjorken and Glashow [6] in order to make quarks and leptons more symmetric. This new quantum number would be carried by a fourth, heavier quark, and would be violated by the weak interaction.

When the psi was discovered, many theories were advanced to account for its maverick behavior. Just a few months after the original announcement, papers had appeared suggesting that the psi (and the similar higher mass state, the $\psi'(3685)$) could be a baryon-anti-baryon bound state[7], a neutral member of a triplet of W bosons[8], neutral Higgs particles[9], and charm-anticharm[10-13]. It soon became apparent, however, that the charm picture was the most reasonable hypothesis. It predicted a complete new spectrum of particles with a charmed quark replacing a normal quark. The psi would be a bound state of $c\text{-}\bar{c}$ (where c is the charmed quark) is the prototype for a set of excited $c\text{-}\bar{c}$ states which are now known as either ψ,ψ', or η_c. There would be mesons made of a charmed quark and a normal quark (or anti-quark), therefore having a non-zero or "naked" charm (as opposed to $c\text{-}\bar{c}$ which has "hidden" charm), and also baryons with at least one charmed quark. At the present time, charmed mesons have been found[14], mostly produced in e+e- collisions, and there are

several candidates for charmed baryons [15,16]. Together, this family of phenomena have so changed our map of the hadrons as to to be classified as the "New Physics".

Once the existence of this new family of particles has been established, there are several opportunities available for increasing our understanding of how charmed quarks (and by extrapolation, other quarks) interact. The obvious way is to just do more charmed particle searches, establishing the exact masses of those particles that have not yet been found. It will also be necessary, however, to obtain detailed information concerning the modes of production and decay. Insofar that it is almost impossible to detect a particle without some knowledge of its decay modes, part of the first goal may already have been accomplished, but in order to achieve the detail desired, one must have a high efficiency for detecting both the decay products of the charmed (either hidden or naked) particle and those particles produced in association with it. This requires a multi-particle spectrometer with a large acceptance and considerable particle identification. Such a device exists at the Fermi National Accelerator Laboratory near Chicago, at the Muon Laboratory, and it was there that the data presented in this thesis was collected. The individual pieces of equipment will be discussed in Chapter 3, while the acceptance characteristics of the complete setup will be covered in Chapter 5.

Neglecting for the moment the peculiar character of this particular setup, what do we wish to measure, and what can we measure? The touchstone of the "New Physics" is still the psi, and the same signature that made it originally stand out so glaringly should enable the experimenter to isolate the psi signal with a fairly small background. Once that signal is obtained, one can measure the vital parameters of the psi itself, viz. its longitudinal momentum distribution (Feynman x or x_F), its distribution in perpendicular momentum (p_T), and its cross section, perhaps as a function of these variables. Since we did this experiment using two different targets, beryllium and liquid hydrogen (LH2), we could distinguish between those events produced with a bare proton or with a nucleus.

The advantage of using the Muon Lab is the ability to measure well the other particles produced in association with the psi. Just the multiplicity of the hadrons, at least according to Carlson and Suaya[17], will indicate if the psi is produced mainly by gluon fusion of by quark-anti-quark annihilation. The psi plus attendant photons give us a handle on the dynamics of the charmonium system, since we would be able to see some of the radiative decays of the chi states and to set limits on how much of the psi signal comes from these decays.

These measurements on particles which were barely suspected to exist just a few years ago are an exciting example of the rapid progress which can be made in high energy physics, both theoretical and experimental.

CHAPTER 2.

THEORY

Since the Greek philosopher Democritus first suggested that there existed a set of basic building blocks for all objects in the universe, there has probably been argumentation about the nature of these blocks. In the last century scientists have considered many different sets of these blocks, starting with the chemical elements and now being currently occupied with quarks and gluons. It is quite possible that these latter are not any closer to being the ultimate constituents of matter than are earth, air, fire, and water, but they are the closest we have now.

As the present alchemical lore has it, all hadrons can be considered as collections of either a quark and an antiquark (mesons) or three quarks (baryons) being held together by gluons. It is this quark content (the "valence" quarks) which is associated with the characteristic qualities of each hadron. The quantum numbers of the four well known quarks (in the most common scheme) are given in Table 2-1. The discovery of the υ and υ' [1] are evidence for a fifth quark, even heavier than the charmed quark. There could of course be

even heavier quarks whose mass is such that they can not yet be seen experimentally. Even the lighter quarks have not been seen as free particles, but there is persuasive evidence that quarks do exist, but confined within the hadrons. A successful theory of the hadrons would necessarily include an explanation of this quark confinement. In addition to the valence quarks and the gluons, each hadron would also contain a cloud of virtual quark -antiquark pairs called "sea" quarks.

There are essentially two basic aspects to working with quarks and gluons as hadrons. First, it is necessary to understand that the interactions between quarks and gluons at short range are due to their color charge. Color is the quantum number associated with the field which provides the binding force between quarks. Quarks have one of three different colors, but since no differences corresponding to color have been observed among the hadrons, the quarks must be in a color neutral state, i.e. "white". The gluons, as vector gauge particles of the color field, form an octet. Since the gluons themselves carry color (as opposed to photons, which do not in themselves carry charge), gluons can interact among themselves, giving rise to a non-linear theory [2]. This theory of the interactions between quarks and gluons through color is often called quantum chromodynamics (QCD), in analogy to the more mundane quantum electrodynamics (QED). If we denote color by roman indices and space time by greek, let q stand for a vector of color quark fields, b for

gluon fields, f_{abc} and g_{abc} be the anti-symmetric and symmetric SU(3) structure contants and define the following terms [3]

$$D_\mu q = \left(\partial_\mu - ig \frac{\lambda^a}{2} b_\mu^a\right) q \tag{1}$$

$$G_{\mu\nu}^a = \partial_\mu b_\nu^a - \partial_\nu b_\mu^a + g f^{abc} b_\mu^b b_\nu^c \tag{2}$$

we can write the basic QCD Lagrangian as

$$\mathcal{L} = \sum_q \bar{q}\left(i\gamma_\mu D_\mu - m_q\right) q - \frac{1}{4} G_{\mu\nu}^a G_{\mu\nu}^a \quad . \tag{3}$$

In order to fix the color gauge, an extra term must be added

$$\Delta\mathcal{L} = -\frac{1}{2\xi}\left(\partial_\mu b_\mu^a\right)^2 + \partial_\mu \phi^{a*}\left(\partial_\mu \phi^a + g f^{abc} b_\mu^b \phi^c\right) \tag{4}$$

where ξ is the gauge parameter and ϕ is a ghost field necessary to remove an unphysical contribution due to the gauge fixing.

Using this Lagrangian implies that working at small distances is not impossible, because as the distances get smaller and smaller (i.e. as the four-momentum transfer squared tends to infinity) the effective

coupling constant tends to 0 [4] and perturbation methods can be employed. As distances get larger, the coupling gets stronger. It is hoped that this is the mechanism responsible for the confinement of quarks and gluons in hadrons.

After we understand the short-range behavior of quarks and gluons, we must then have some idea of how these constituents are arranged in ordinary hadrons. This problem subdivides itself into two others: 1) what is the distribution of quarks and gluons in the hadron as a function of the longitudinal momentum fraction (Feynman x or x_F), and 2) how do free quarks and/or gluons being expelled from an interaction turn themselves into ordinary hadrons - the so-called "dressing" functions - as they try to clothe their bare color charge. As these problems involve long-range behavior, they are not very amenable to solution using only QCD theory methods. The result is that there are many different quark distributions available in the literature [5]. Deep inelastic lepton-nucleon scattering form factors (e.g. $\nu W_2^{ep}, \nu W_2^{\nu p}$ etc. which are derived from the reactions like $ep \rightarrow e+$anything and $\nu p \rightarrow \nu +$anything) are available for certain kinematic regions and can provide information on the charged contents of the nucleon when considered with the various sum rules and isospin invariance properties of the nucleons. There are no pion targets available, however, and the quark distribution functions for mesons could be regarded as being as much art as science. The same applies

to the gluon functions for both mesons and baryons.

The calculations I will quote in general do not try to dress the charmed quarks. The assumption is that charmed particles will follow the same distributions as the charmed quarks do. One exception is Carlson and Suaya [6] who explicitly demand that the pair of charmed quarks which eventually give rise to a psi must be in a colorless singlet at each stage of the interaction.

To produce a bound state of $c\text{-}\bar{c}$ such as the psi is not easy. Various possible ways are shown in Fig. 2-1. Cross sections for the various production mechanisms are of course dependent upon the quark and gluon distributions, especially Fig 2-1b, which depends quadratically upon the very small and not very well known charmed sea. It seems, however, that the major contributions must come from some combination of gluon fusion (2-1d) [6,7] and a Drell-Yan-like quark fusion diagram (2-1c). (We note that a one gluon diagram like 2-1c cannot produce a color singlet and that a soft gluon must leak off to produce a physical particle. 2-1a does not have this problem, but it has a very small cross section [8]). The ratio of the contributions from these two processes is a function of incident particle and energy, and x_F in the following manner: 1)more quark fusion is present when using a meson or antiproton beam since they contain antiquarks, 2) gluon fusion drops off more rapidly than quark fusion as x_F approaches one, and 3) at high energies, gluon fusion rises more

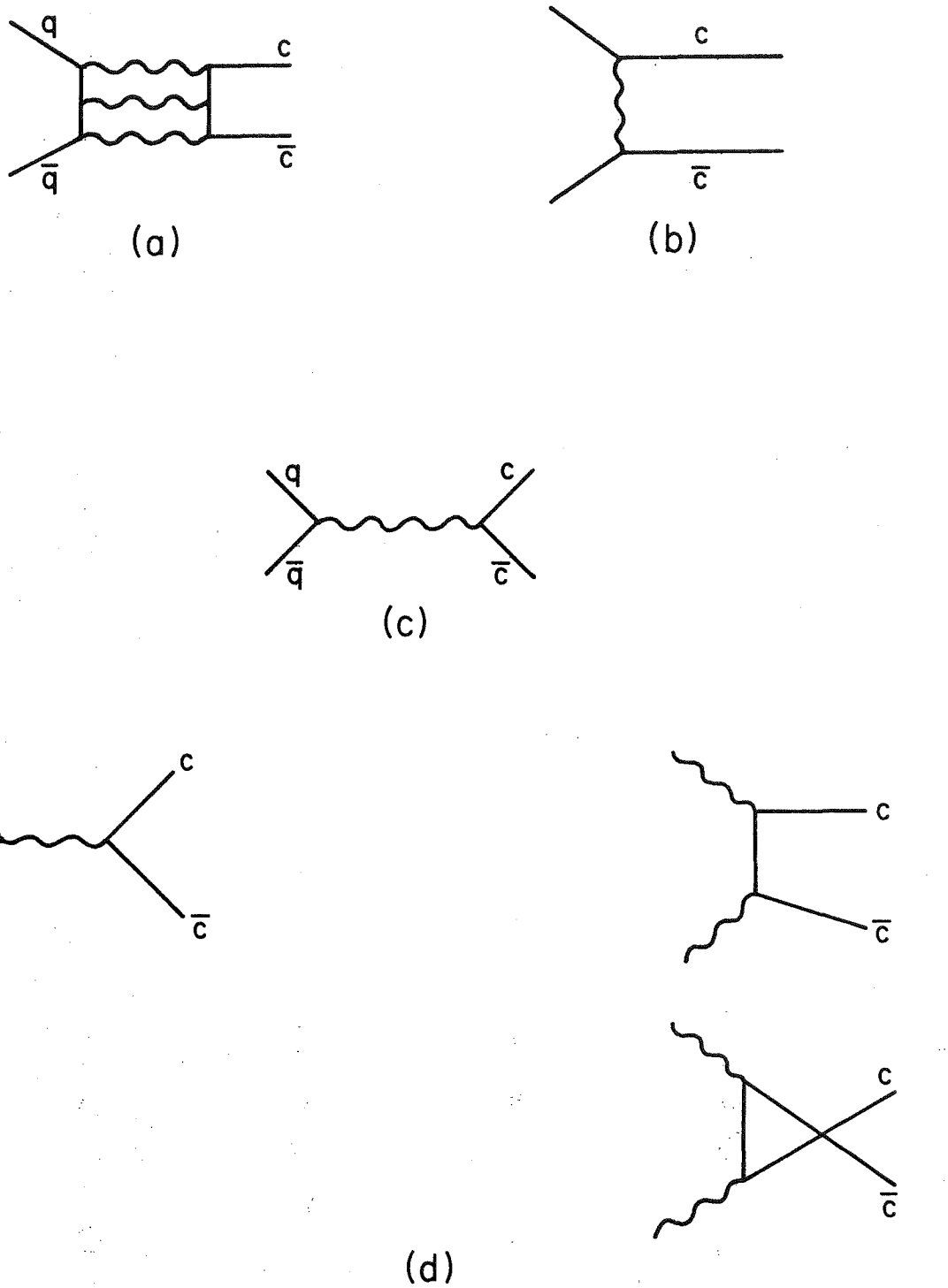

Figure 2-1. QCD processes for production of charmonium.
(a) quark fusion,
(b) charmed quark pairing,
(c) quark fusion,
(d) gluon fusion.

rapidly than quark fusion.

Calculations of the rate of production for cc result in the total cross section for all charmed states. To make an estimate of the production of a particular state in the mass region below the threshold for the production of naked charm, it is necessary to make an arbitrary decision allocating the cross section among all the states. A possible alternative is the approach used in reference 6. Their calculations give definite predictions concerning the rates of production of the various charmonium states. They unfortunately require the charmonium wavefunctions as input, however. They find

$$\Gamma\left(gg \to {}^3P_o\right) = \frac{2}{3}\, 9\, \alpha_g^2\, m_q^{-4} \left|\frac{d\phi(o)}{dr}\right|^2 \tag{5}$$

$$\Gamma\left(gg \to {}^3P_1\right) = \frac{1}{15}\, \Gamma\left(gg \to {}^3P_o\right) \tag{6}$$

$$\Gamma\left(gg \to {}^3P_2\right) = \frac{4}{15}\, \Gamma\left(gg \to {}^3P_o\right) \tag{7}$$

where $\alpha_g = 0.19$, $\lambda = 0.2029$, $m_q = 1.84$ Gev, and ϕ is the radial wavefunction.

In finding the charmonium wavefunctions, a common approach is to cite the apparently heavy mass of the charmed quark and use non-relativistic potential theory, possibly with first order

relativistic corrections. Such a potential would probably tend to look Coulombic at small distances and also to have a term to force confinement at large distances [2]. Such a potential is [6]

$$V(r) = -\frac{4}{3}\frac{\alpha_s}{r} + \lambda r \quad . \tag{8}$$

Other authors go so far as to just use a harmonic oscillator potential because of ease in calculation [2]. The parameters in these potentials can be fitted using the leptonic branching ratios and the mass splitting of the ψ and ψ'.

We present the known charmonium spectrum in Fig. 2-2, indicating both the normal name and the spectroscopic designation. The two states X(2.830) and χ(3.455) have been suggested as candidates for the 1^1S_o and 2^1S_o states, but there are serious difficulties with this assignment (see reference 8 for a novel counterproposal). What we can observe are those transitions which are allowed by charge conjugation parity (where $C=(-1)^{\ell+s}$ and both the and have C=-1) between the various chis and the psi. We can also see the charged tracks associated with the psi. Unfortunately, experimental limitation raises its ugly head here - we cannot well resolve the various chi states - that problem must be left for a later day and an improved experiment, however, our results for all the chis lumped together will be presented in Chapter 5.

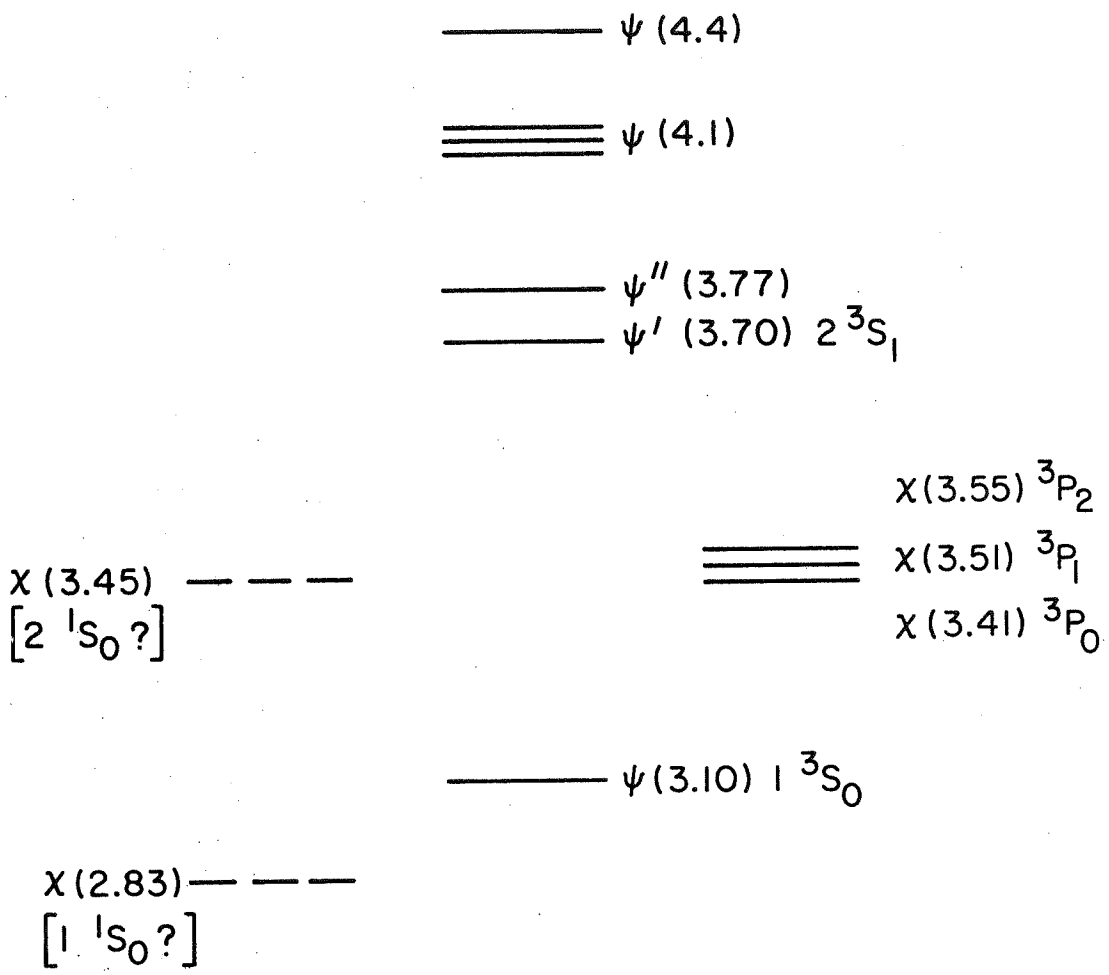

Figure 2-2. The charmonium spectrum.

	Q	I_ω	S	C	Spin
u	2/3	1/2	0	0	1/2
d	-1/3	1/2	0	0	1/2
s	-1/3	1/2	-1	0	1/2
c	2/3	1/2	0	1	1/2

Table 2-1.

Quark Quantum Numbers

Chapter 2 References

1. S. Herb et al., Phys. Rev. Lett. 39, 252 (1977)

W. Innes et al., Phys. Rev. Lett. 39, 1240 (1977)

W. Innes et al., Phys. Rev. Lett. 39, 1640 (1977).

2. V.A. Novikov et al., Phys. Rep. 41C, 1 (1978).

3. M. Gell-Mann and Y. Nee'Man, The Eightfold Way, Benjamin, 1964.

4. H.D. Politzer, Phys. Rev. Lett. 30, 1346 (1973).

5. R. Field and R.P. Feynman, Phys. Rev. D15, 2590 (1977).

G. Farrar, Nuc. Phys. B77, 429 (1974).

6. C.E. Carlson and R. Suaya, Phys. Rev. D18, 760 (1978).

7. M. Gluck, J.F. Owens and E. Reya, Phys. Rev. D17, 2324 (1978).

8. H.J. Lipkin, H.R. Rubinstein, and N. Isgur, Wisconsin preprint, WIS-78/23 PH.

CHAPTER 3.

EQUIPMENT

The data presented in this thesis was collected at the Muon Laboratory of the Fermi National Accelerator Laboratory (Fermilab). Figure 3-1 shows a schematic drawing of the equipment. The equipment in this lab originally came from several institutions interested in doing high energy physics with an incident beam of muons (hence the name). Oxford supplied hodoscopes of plastic scintillator and a multicelled Cerenkov. The University of Illinois and Harvard University provided spark chambers and proportional wire chambers (PWCs or MWPCs). The University of Chicago supplied spark chambers, MWPCs, and the online computer used for recording the data on magnetic tape.

The unique feature of the Muon Lab is the Chicago Cyclotron Magnet (CCM). As the name indicates, this magnet was originally used in Fermi's 450 Mev cyclotron at the University of Chicago. Transported to its present site at the beginning of construction on the Muon Lab, it has become the center of Fermilab's co-ordinate system, as it weighs about two thousand tons and is anchored to

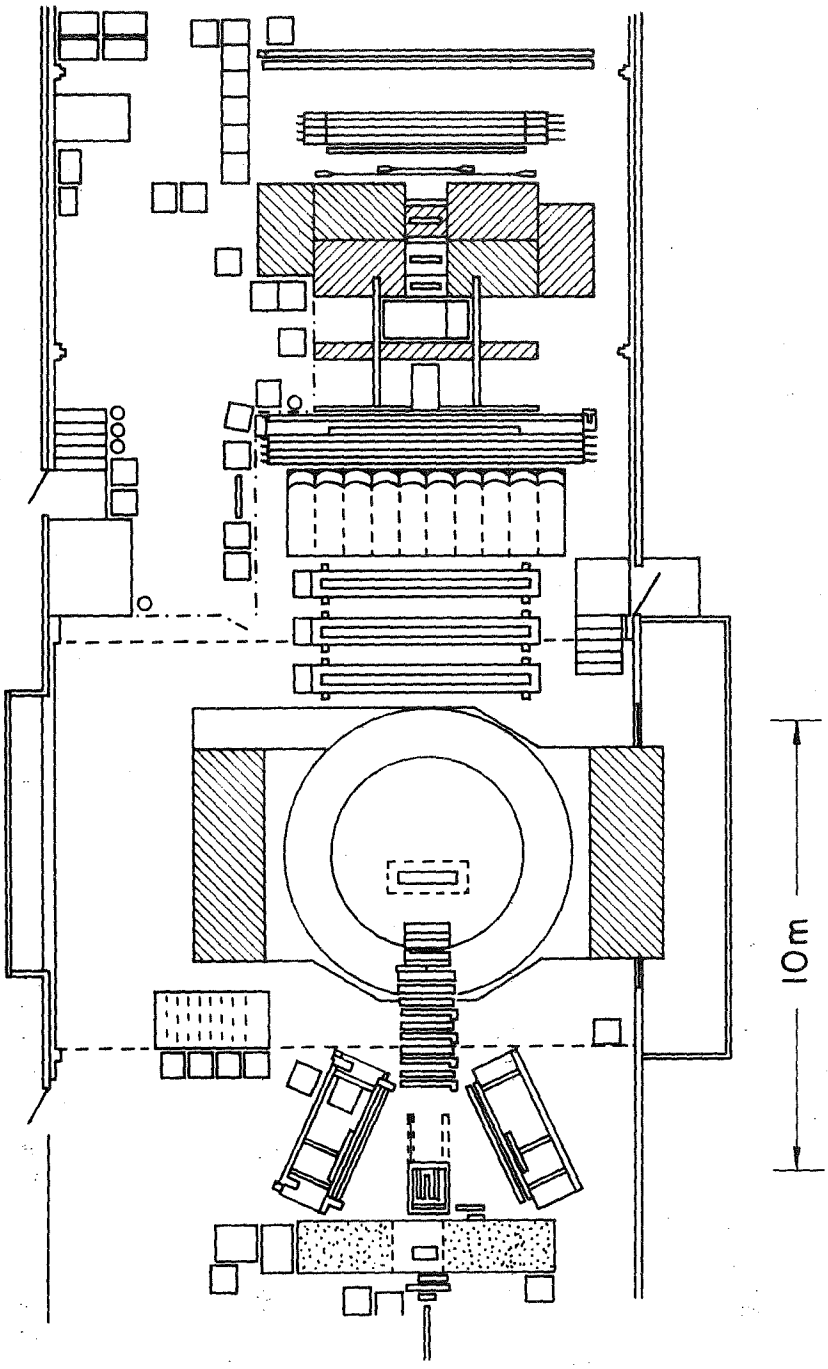

Figure 3-1. The muon lab.

bedrock with 80' concrete pilings. This experiment also used the CCM as its co-ordinate system, the origin being the center of the magnet gap and the pole faces. The positive y-axis was vertically upward while the positive z-axis was in the direction of beam travel. We operated the magnet as a particle spectrometer by placing proportional and/or spark chambers on either side and observing the deflection of particle paths. As the CCM has a pole face of 4.32 m, a gap of 1.29 m, and it was operated at a field of 14.2 kilogauss (an excitation of about 4100 amps and 2MW), a beam particle of 215 Gev/c momentum would display a deflection of about 10 milliradian. A particle of 5 Gev/c or less, however, will never reach the set of wire chambers on the outgoing side (downstream) of the magnet. This is the basis for the acceptance characteristics of the apparatus as a function of momentum along the beam direction.

The various sets of spark chambers and proportional wire chambers have been described fully elsewhere [1], so only an abbreviated description will be given. The planes upstream of the CCM were all PWC's and came in three varieties: 1) beam line chambers, 2) University of Chicago 1m x 1m planes, and 3) University of Illinois 0.8m x 0.8m planes.

There were originally six PWC's placed along the beamline which were used to determine the x and y co-ordinates of beam particles (4 x-chambers and 2 y-chambers). See Fig 3-2. The active area was 8" x

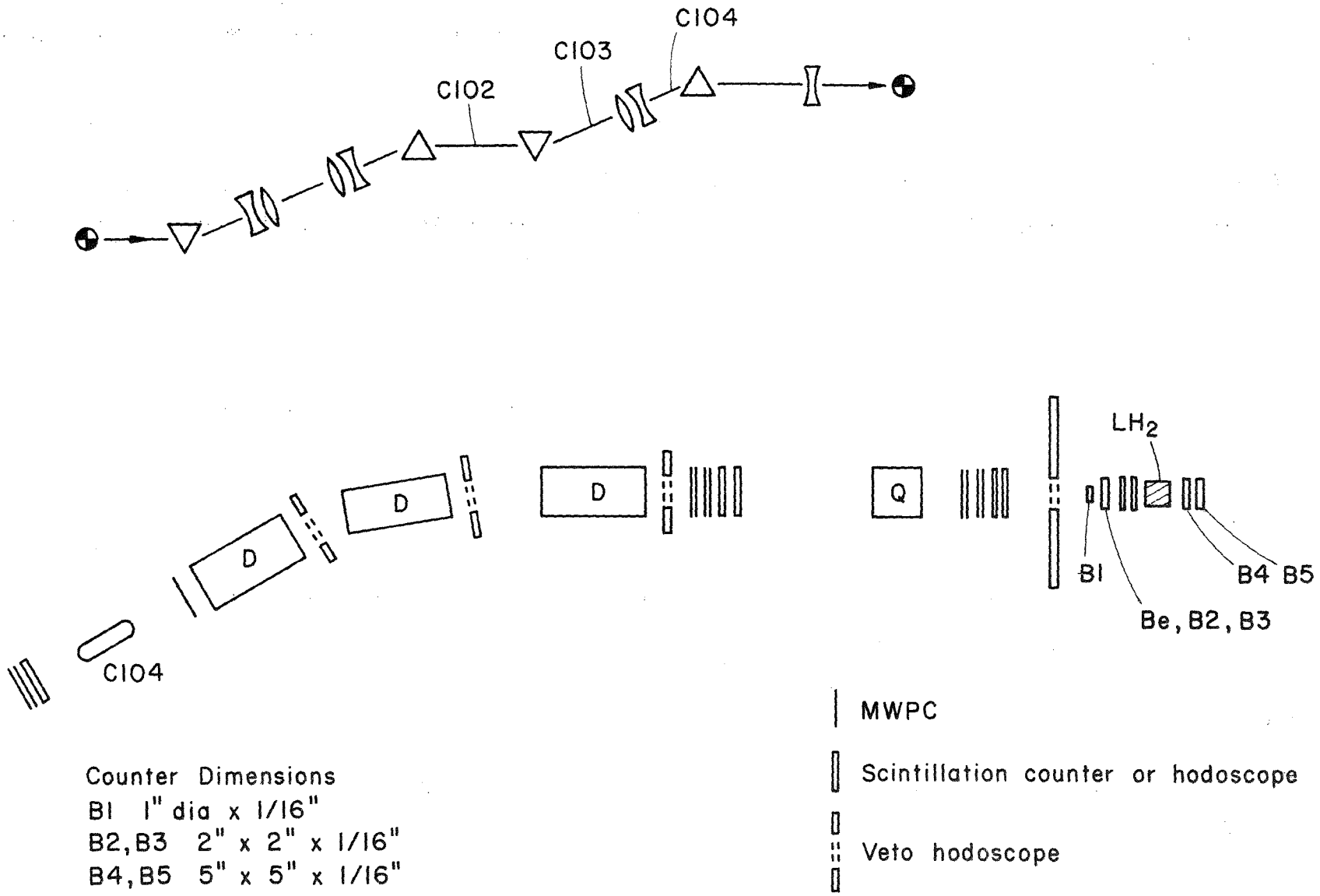

Figure 3-2. Beam line and target regions.

8" and the wire spacing was 0.0825". Five of the six planes were actually double planes, i.e. there were two sets of wires with 0.0825" spacing placed close to each other and then staggered by half a wire spacing. There were also six scintillation hodoscopes consisting of 8 elements 6" x 0.075" x 0.025" each, adjacent to the PWC planes. There were only five double planes because one set of wires and one hodoscope had to be physically removed to provide room for a Cerenkov detector. There also existed veto scintillators, i.e. scintillators with holes in them where beam particles were intended to pass. A signal from one of these counters meant an additional particle was present which would confuse the entire event. In addition to 3 such sets in the beamline, the entire upstream end of the lab was covered with a veto-wall. The three Cerenkov detectors in the beamline were converted sections of beam pipe filled with helium at low pressure and fitted with mirrors and RCA 33000M photomultipliers. Due to various and sundry reasons, none of this equipment consistently worked for the complete length of the data taking. As a matter of fact, the same could be said of almost every piece of equipment in the Muon Lab, from the lavatory fixtures to the data logging computer.

The Chicago 1m x 1m PWC's and the Illinois 0.8m x 0.8m PWC's were used to determine the trajectory of outgoing particles before they were deflected by the CCM. The 0.8m x 0.8m chambers were especially

useful for finding the curvature of tracks which were too low in momentum to reach downstream of the CCM. The Chicago 1m x 1m planes consisted of 5 x-y pairs with a wire spacing of 1.5mm and an active region of 1m square (of course). One of these pairs was actually anchored at the mid-line of the CCM. The Illinois 0.8m x 0.8m chambers, originally 10 planes in number, had a wire spacing of 0.125" and were turned into u or v planes (i.e. planes with a non-zero tilt relative to the x-y planes, in this case +/- 26 degrees) by the novel expedient of physically tilting an entire chamber to the desired angle. They were used, when they were working, to remove the ambiguities inherent in trackfinding with only x-y chambers, and, since they were actually on the edge of the magnet, to follow the tracks as they began to curve.

All of the chambers upstream of the CCM were proportional chambers since the high forward-going particle density required both good spatial and time resolution and short dead time, but allowed small area. Conversely, all the chambers downstream of the CCM were spark chambers. The University of Chicago provided three modules of four planes covering 4m x 2m and with a wire spacing of 1.25mm. Each module contained planes in the order UXXV where the u-v tilt angle was +/- arctan(0.125) to the vertical. These chambers were read out using an individual capacitor for each wire which was then connected to the input of a shift register. The live time for these chambers was about

10 microseconds (as opposed to roughly 100 nanoseconds for the 1m x 1m PWC's).

The other spark chambers, originating at Harvard, were either 6m x 2m in area or 4m x 2m, and used a magnetostrictive wand readout system. Wire spacing was 1.25mm for both sets. The 6m x 2m set contained 8 planes arranged in the order UXUXVUXV (where again the u-v tilt angle is +/- arctan(0.125)). The 4m x 2m set was arranged in the order UXXVUVUX. The 4m x 2m set of Harvard chambers was downstream of a 2.2m thick pile of iron (which originally formed the Rochester cyclotron magnet). They were used to help determine which of the downstream tracks were actually muons, and therefore these chambers were usually termed "the muon chambers" to distinguish them from the 4m x 2m Chicago chambers.

A series of four scintillation counter hodoscopes downstream of the iron hadron absorber were also used to find muons. The most important of these hodoscopes, the P hodoscope (see Fig. 3-3), was configured in the so-called "Bow-tie" pattern so that it could be used in the event trigger logic. In order to remove the background in the di-muon sample due to in-flight decays of pions, the P hodoscope had areas removed to eliminate muons with a small value of p_T/p_L. This preferentially accepts muons coming from the decay of a higher mass object. It is also possible to enhance signal/background by requiring that muons be found in opposite quadrants of the hodoscope. The

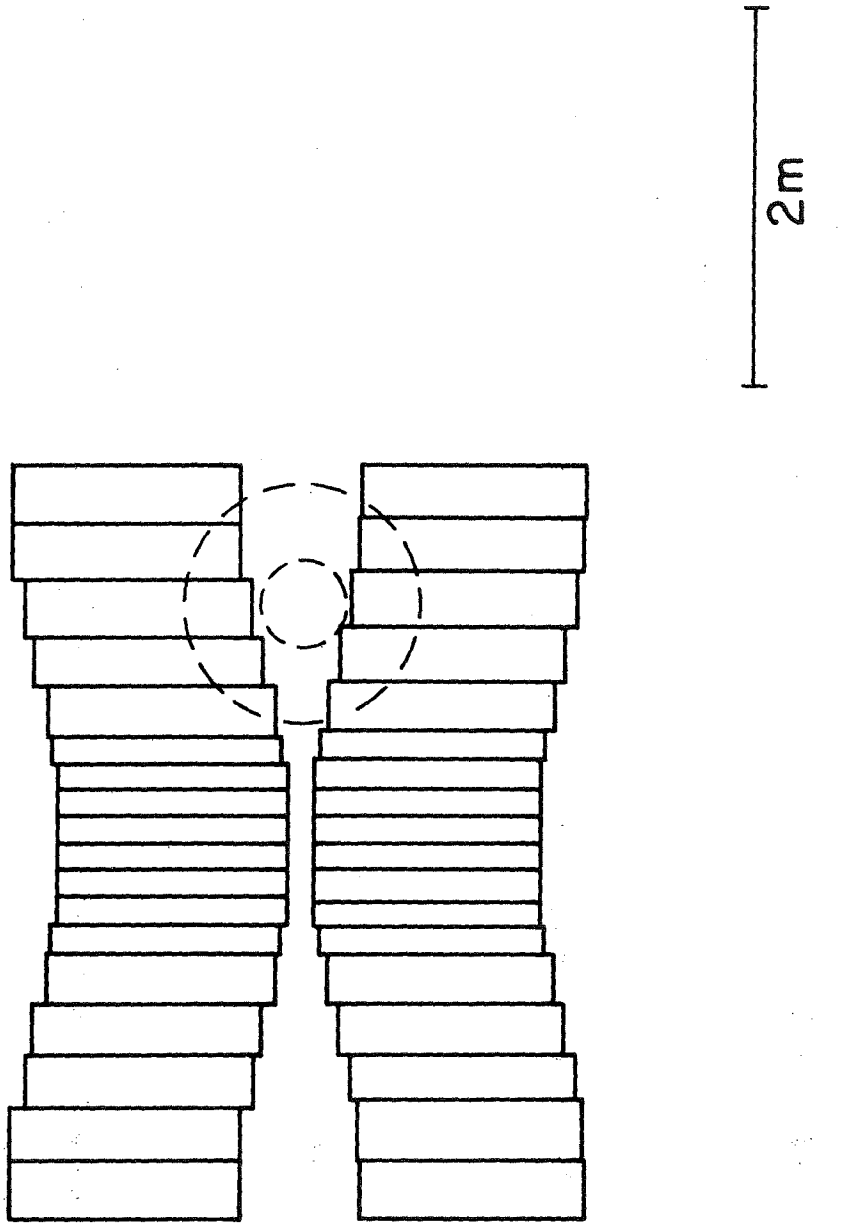

Figure 3-3.

dashed circles in Figure 3-3 show how the "Bow-tie" configuration works. The center of the circles corresponds to the position of a particle with a momentum of 25 Gev/c, and the two cirles represent the smearing due to a p_T of either 0.2 or 0.6 Gev/c. We see that only those particles with the larger value of p_T will hit the hodoscope.

Two large hodoscopes located upstream of the hadron absorber and labelled G and H, were oriented to separate tracks either vertically or horizontally, respectively. They roughly covered the same area as the spark chambers. Information from these hodoscopes was used in the analysis routines to eliminate spurious tracks.

The target was segmented into two parts: 2.6cm of Be and 46cm of liquid hydrogen. These combined to give a total length of 7.75% of one interaction length, 4.25% for the Be and 3.5% for the LH2. The LH2 was contained in a 3.2 cm diameter cylindrical flask. The Be was in the form of rectangular plates strapped together to give the correct thickness. The transverse dimensions were 3.2 cm x 3.6 cm. A set of scintillation counters was situated to distinguish interactions occurring in the Be or the LH2. A circular counter with an air light guide between the scintillator and the photomultiplier tube was placed before both targets, two counters were between the two targets, and the LH2 was followed by another pair of counters. In the experimental nomenclature, the signals from these counters were B1,B2,B3,B4, and B5 (see Figure 3-2).

The major decision paths for the control and trigger logic are shown in Fig. 3-4. The functions can be roughly described as 1) to determine when an event of interest had occurred, 2) to trigger the various pieces of equipment in the lab which required a more selective trigger than just a beam particle, 3) to enter the data into registers, and 4) to inform the data logging computer. It is really only the first of these chores which has any interesting facets. The various original design criteria of the experiment are embodied in the final merging of the various sub-triggers: 1) 2 mu = dimuon triggers, 2) 1mu.P = diffractive excitation charm search, and 3) LMP = low-mass proton (diffractive excitation again, but over a different mass region which was intended to allow a superior measurement of the A1,A2,A3 meson region to be made). Ideally the trigger circuitry would have allowed for the merging of any given combination of the three sub-triggers, but trigger rates were such that it was normally run set to 2mu+(1mu.p) and then gated with a coincidence circuit during the last 5 msec of the beam spill to pass LMP triggers.

In order to help identify the types of hadrons coming from an interaction, an 18 cell gas Cerenkov counter was placed between the 4m x 2m WSC's and the 6m x 2m WSC's. The working medium was 99.99+% pure nitrogen at atmospheric pressure. The cells were 1.8m long and were arranged two high by nine wide to cover the same area as the spark chambers. Each cell had a mirror to focus the light on a 5" diameter

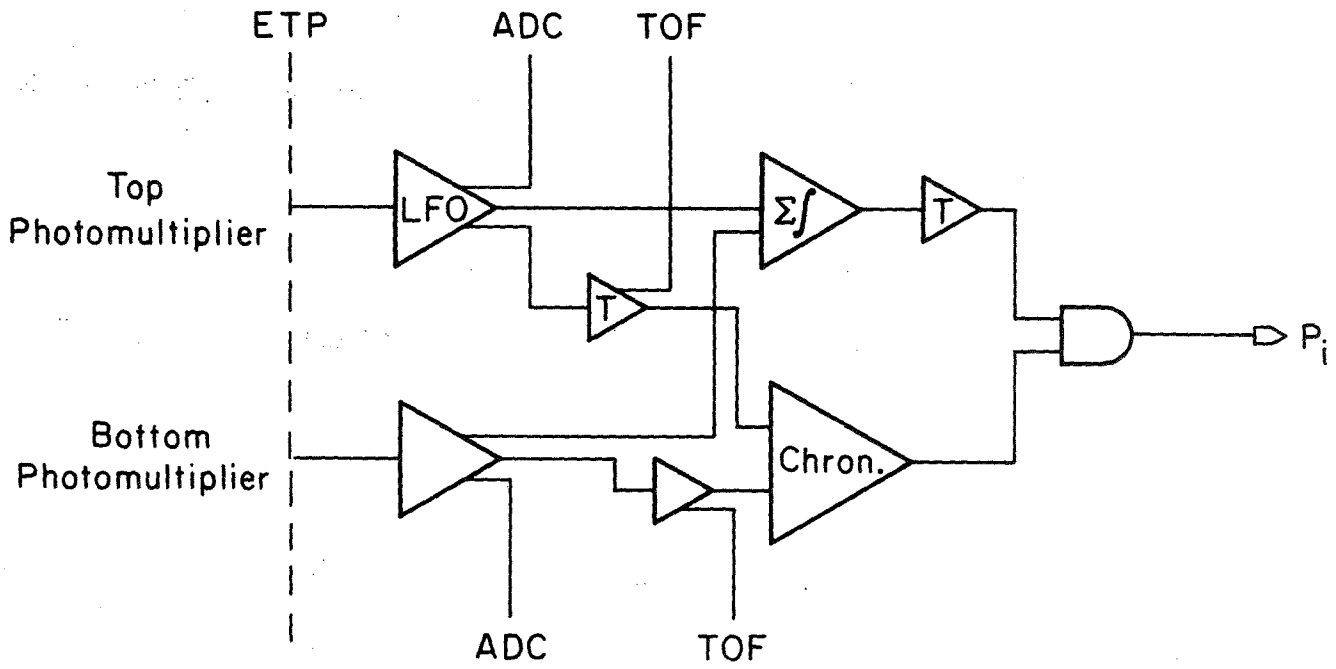

Figure 3-4. Electronics diagrams.
(a) Recoil logic for single channel.

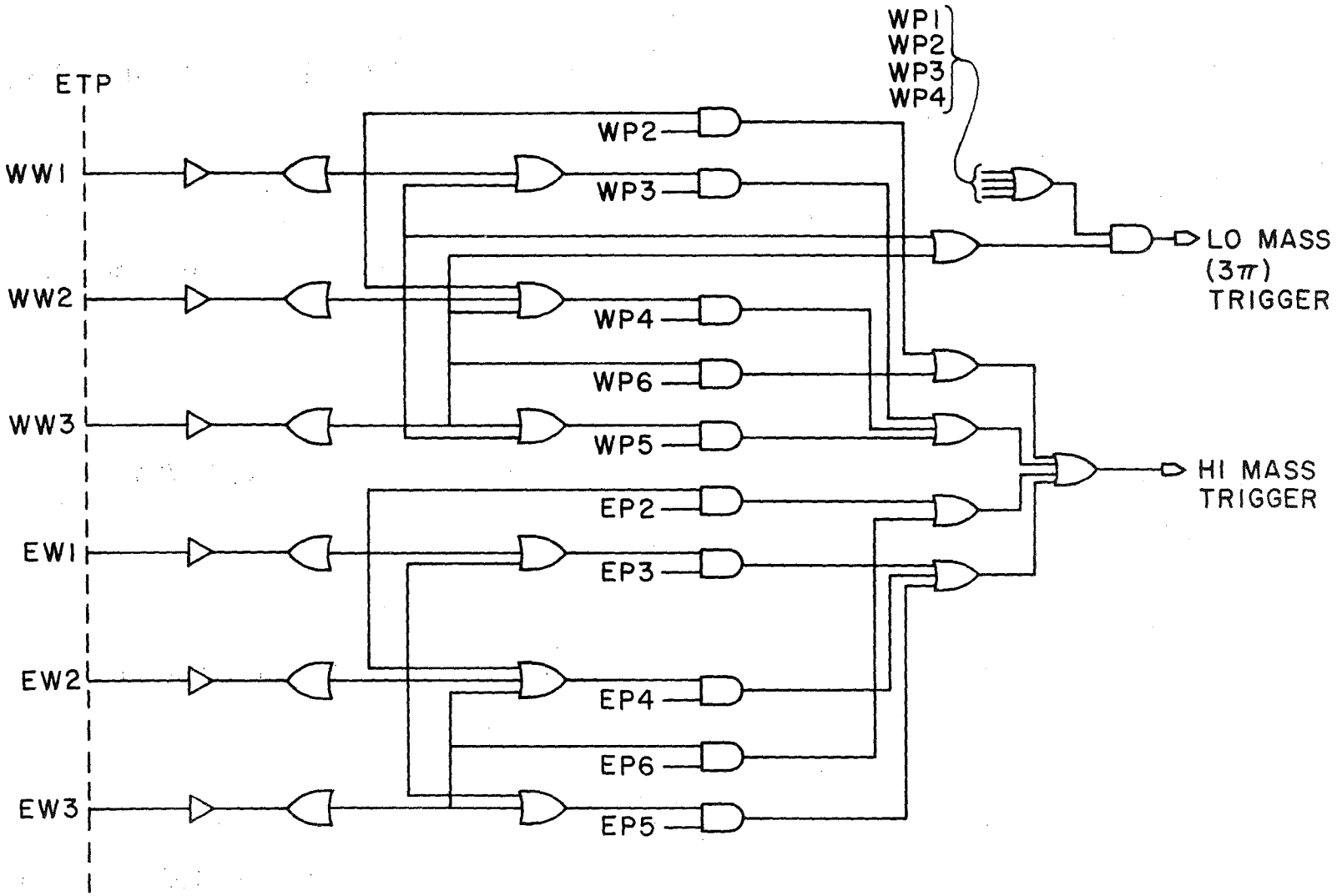

Figure 3-4. Electronics diagrams.
(b) Recoil MWPC "AND" counter logic.

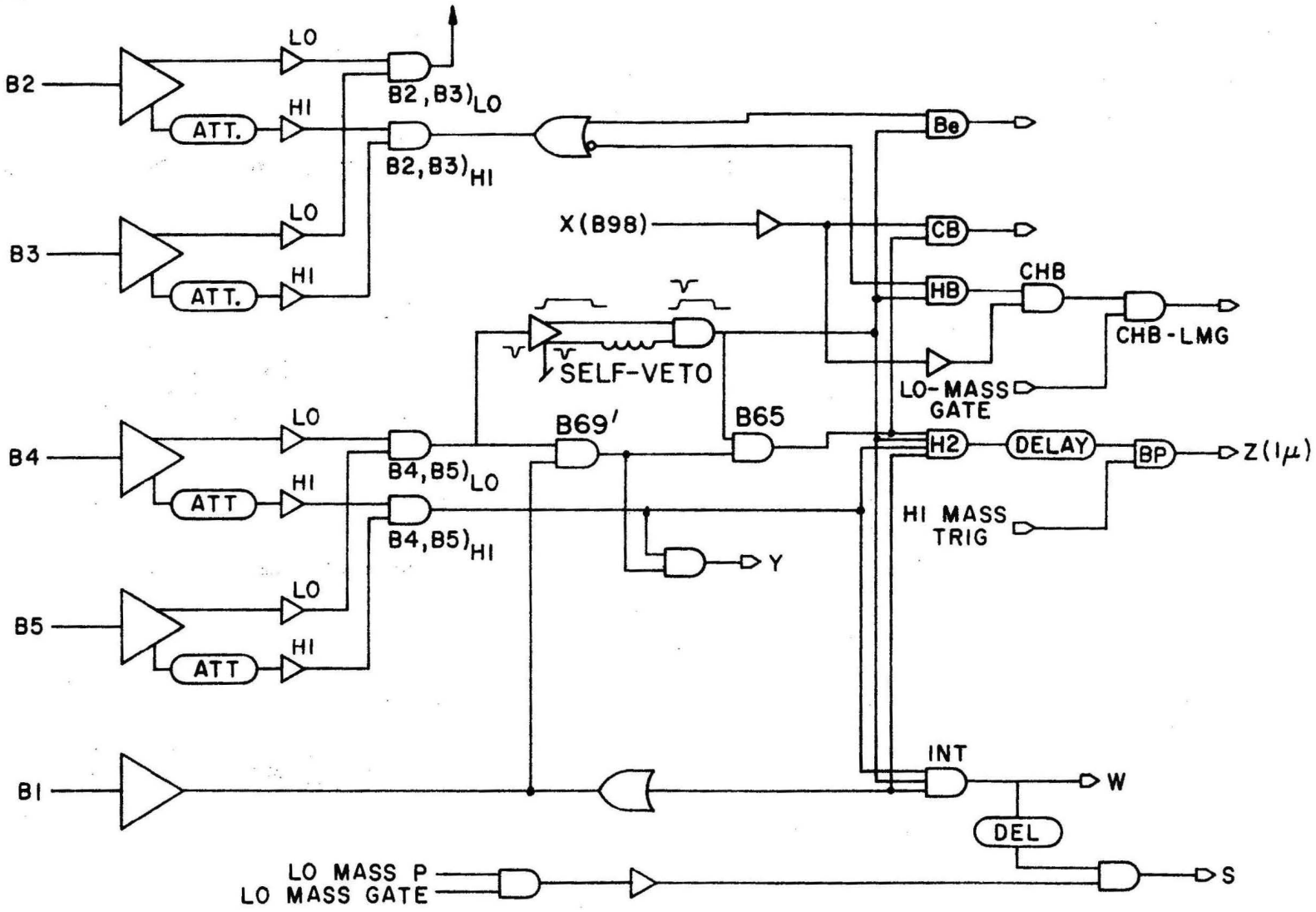

Figure 3-4. Electronics diagrams.
(c) Beam logic.

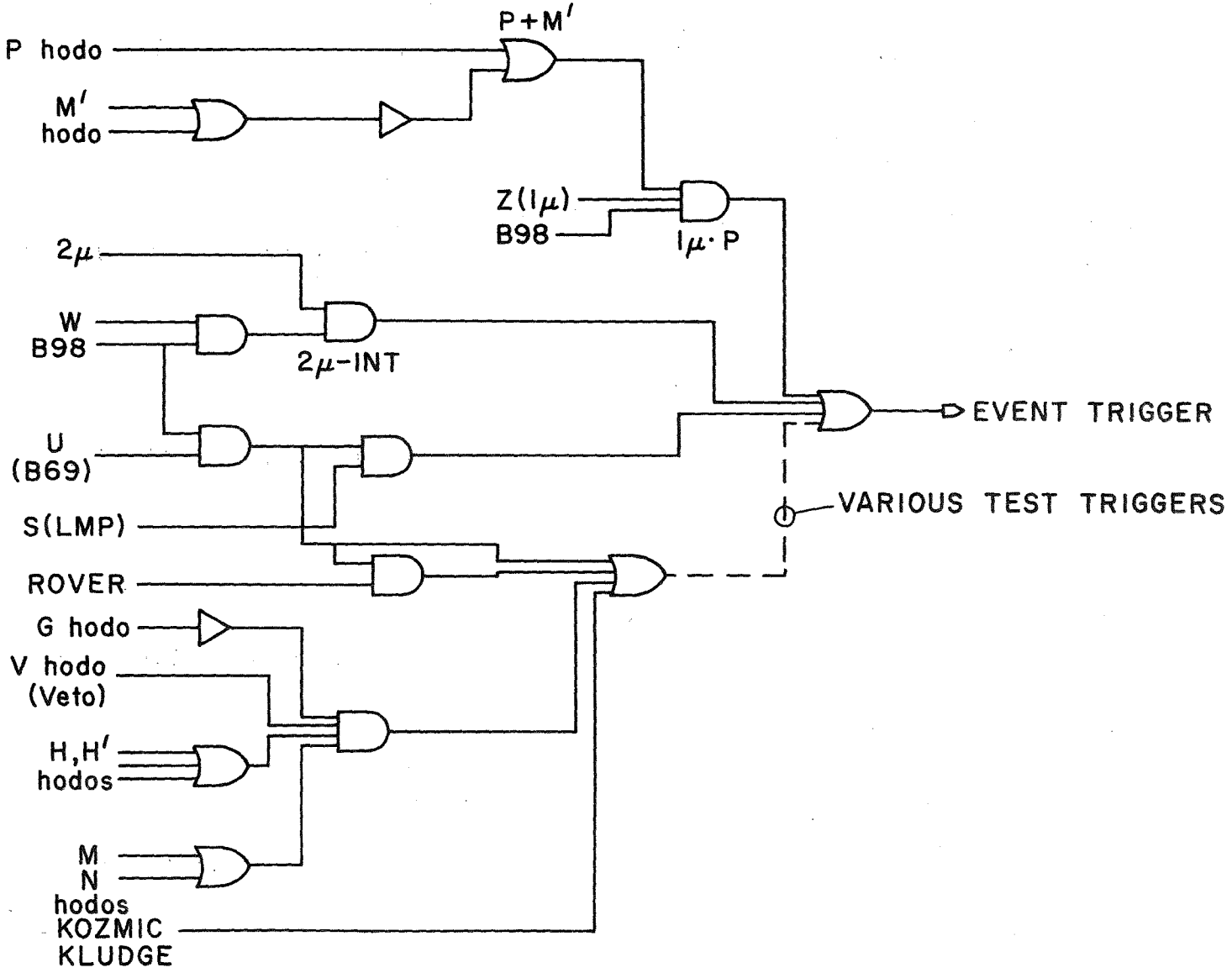

Figure 3-4. Electronics diagrams.
(d) Trigger logic.

RCA 4522 photomultiplier tube. Due to the low overall efficiency of the Cerenkov (the average number of photoelectrons for a minimum ionizing particle was in the range of 2-3), complete pion/kaon separation was not feasible. It could be used, however, to provide an enhanced sample of kaons. At 21 Gev/c, just before the threshold for production of Cerenkov light by kaons, the pion contamination would be about 33%, averaging over all the cells. At any other momentum, the contamination would be worse. Below 6 Gev/c there is no Cerenkov light from pions, while at about 42 Gev/c, a kaon will emit 75% of the light available from a minimum ionizing particle.

In order to detect photons, an array of lead glass counters belonging to Tufts University and University of Massachusetts was used. Originally 10 blocks high by 8 blocks wide, during use in the Muon Lab only 76 blocks were operational, the defunct units being replaced with ones from the top and penultimate rows. The blocks themselves were constructed of Schott Optical SF-2 glass and measured 6.35cm x 6.35cm x 58.4cm with the long dimension being aligned parallel to the beam. This type of glass has an index of refraction of 1.65 and is 51% PbO by weight, with one radiation length being 2.76cm. Thus each block was 21 radiation lengths long and would contain more than 98% of a 20 Gev shower [2]. Calibration of each lead glass block-Amperex XP-2020 phototube combination was performed once each data run (roughly 2-3 hours) using Monsanto MV5222

light-emitting diodes attached to the front of each block. The pulse heights, as measured by analog-to-digital converters (LeCroy model 2248), were recorded using a CAMAC unit connected to a Digital Equipment Corporation PDP-11 computer.

The overall data logging, including some of the data originally recorded by the PDP-11, was done with a Xerox Data Systems Sigma-3 16 bit computer equipped with 64K words of memory and a 1.5 Mbyte disk. The master data acquisition program was originally written at the University of Chicago for use with the muon scattering experiment, E98 (CHIO collaboration), and was slightly modified for use with the re-configured apparatus. Upon receiving an event trigger interrupt, the computer would interrogate the CAMAC system to retrieve the data, which was then written to a buffer on the disk. At the end of the beam spill (roughly 1 sec long every 12 seconds) or in the event of a full buffer, the data acquired was written to one of the two 9 track 800 bpi tape drives. This system also allowed considerable online monitoring of equipment performance. Unfortunately, the Sigma-3 suffered a catastrophic failure near the end of the experiment, and after about a week of fruitless repair efforts and some heroic labor on the part of Michael Shupe in writing a new acquisition program, the PDP-11 was pressed into service as the main data logging computer. A tactical decision was made at this point, however, and data taking was restricted to only diffraction events whcih were useless for finding

psis.

During the two months (600 hours) when beam was on target, we received 4.1×10^{10} pions resulting in 129K dimuon triggers. The processing of this data will be described in the next chapters, but for an overall timetable of the experiment, see Table 3-1.

E369 Timetable

Psi discovered	November 1974
First E369 proposal (P369)	December 1974-January 1975
P369 Test Run	April 1975
Second Proposal	October 1975
Experimental setup period	January-June 1977
Experimental run	July-August 1977
Data Analysis	August 1977 - August 1978 - ...
	First Psis Reconstructed — December 1977
	First Chis Reconstructed — June 1978
Total Experiment run time	600 hrs.
	4.1×10^{10} vs. 2×10^{11} for proposal
	2.7×10^{10} for 2mu triggers

Trigger Type	No. Triggers
2MU	309K
1MU.P	129K
LMP	389K

Table 3-1.

Chapter 3 References

1. S. Pordes, thesis, Harvard, 1976

V. Bharadwaj, thesis, Balliol College, Oxford, 1977

R. Hicks, thesis, University of Illinois, 1978

T.A. Nunamaker, Nucl. Inst. Meth. 106, 557 (1973)

T.A. Nunamaker and D. Turner, Nucl. Inst. Meth. 113, 445 (1973).

2. M. Shupe, thesis, Tufts University, 1976.

CHAPTER 4.

DATA PROCESSING

The problem of extracting physics from our over two hundred data tapes occupied several people for longer than a year, and was carried out at the University of Illinois, Oxford University, and Fermilab. It was first necessary to discover the position of all our detectors in real space, after which we could convert our measurements in fiducial space to real space and try to convert hits in the MWPC's, WSC's, and scintillation counters into trajectories of particles. Since alignment depended on using particle trajectories to align with, the initial stages were a bootstrap type of procedure.

To add to the difficulties were those little foul-ups which are an inherent part of any physical experiment, especially one conducted under such frantic operating conditions as this one. Two such incidents which might not possibly be classified as "little", as they affected all the data, caused some worry before they were remedied. The first was an error in the wiring of the 0.8m x 0.8m MWPC's which caused the signals from every eight wires to be read out in inverted order. Once noted, this was fixed by a straightforward software

patch. The second was another hardware problem, this one concerning all the large Harvard spark chambers. Their long magnetostrictive wand readouts displayed local nonlinearities in the speed of sound to such an extent that track finding was not very efficient. A several parameter piecewise linear fit corrected this problem, but as the non-linearities changed with time (or temperature, or the phase of the moon - we never figured it out completely) it was necessary to re-fit the corrections every data run. Most of this fitting was done at Oxford.

Once the alignment has been done, it is possible to refine and tune the trackfinding programs. At Illinois, the problem was approached by using a fairly simple basic algorithm. One would pick two different planes (either spark chamber or proportional chamber) called seed planes, and then take all possible combinations of hits in the two planes to form track candidates. One would then search the other planes for hits in the neighborhood of the track candidate (called the road). The refining and tuning consisted of inserting cuts which would lower the number of candidates it was necessary to investigate, and also determining the minimal set of criteria to define a good track. A minimal set of such cuts and criteria were the parameters to determine the road width and the minimum acceptable number of sparks in x and y plus a maximum acceptable chi-squared for a fit of the sparks to a straight line.

When no tilted planes were available to correlate tracks in x and y, as upsteam of the CCM, trackfinding was necessarily an independent process in the two dimensions. This resulted in what were called either x or y views, which had to be associated using some other source of information such as downsteam tracks. Downstream of the CCM, track candidates were first found in the x-chambers. Using these candidates, u and v co-ordinates were transformed to y co-ordinates and were used to trackfind in y using a somewhat different algorithm in which all the y co-ordinates were projected to a single z co-ordinate. The distribution of the hits in y was then examined for clumps which would indicate associated hits. Associated hits in x,u, and v were then fit to track parameters using a least squares routine. Sparks could be dropped from the fit until the chi-squared passed minimum requirements or there were insufficient sparks left to pass the minimum spark number cut.

The efficiency of this process was obviously dependent upon the efficiency of the chambers. Tests to reveal the efficiency of the pattern recognition by techniques such as inserting a false track and then trying to find it will thus produce a spuriously high efficiency. Gains may be made in recovering minimal tracks by relaxing some of the cuts but one pays for this with an increasing number of false tracks. This is especially true in that region of the chambers where the non-interacting beam particles pass. Due to the long live-time of the

spark chambers and their regular spacing, a grid of closely packed sparks is present which results in a large number of false tracks all sharing the same sparks. It was thus necessary to remove tracks which shared a high proportion of their component sparks with another track of higher quality. Even after this, legitimate tracks were present which were not associated with the event itself but were out-of-time tracks. These were eliminated by requiring that the scintillation counters along a track also fire. These measures help to remove bad tracks, but if track standards are dropped sufficiently, sheer combinatorials from all the sparks will swamp the track finding process. After the most judicious selection of trackfinding parameters, the downstream trackfinding efficiency was probably averaging greater than 90%.

Trackfinding done at Oxford used a completely different algorithm which was originally developed for use with a muon scattering experiment. Relying mainly on the Harvard 6m x 2m chambers which were set very close together in z, a search was made in x for clumps of sparks which were then used as the basis for a trial chi-squared fit. A much more complete description of this is given in the thesis of S. Pordes. It was this set of tracks processed at Oxford which was used to select the actual psi sample presented in this sample.

The vertex of each event was found using the upstream views in x and y. It was first found independently in x-z and y-z by iteratively finding a weighted position of closest approach and eliminating tracks not passing sufficiently close to the trial vertex. When the fit of the trial vertex was acceptable, a check was made to insure that none of the tracks thrown out during the trial fits would pass near the vertex. If some did, they could be added to the fit. Upon finding a vertex in both x and y (or not finding, as the case may be) an overall z postion for the vertex was determined by averaging the two views.

Once the vertex has been found, track parameters can be recalculated demanding that they pass near the vertex. With this constraint and muon identification from the P-hodoscope, dimuon mass combinations are easy to calculate. An early dimuon mass spectrum using the Oxford vertex finder is shown in Figure 4-1. Taking all dimuon events in the mass region 2.9 Gev/c^2<$M_{\mu\mu}$<3.3 Gev/c^2, we can then vary all the different ingredients which were involved in determining the mass (e.g. track parameters and vertex postion) and force them to values which will give a mass of 3.098 Gev/c , i.e. the psi. As we know the uncertainties of all these ingredients, we can then form a chi-squared for this fit.

The lead glass counter was used to find the photons associated with each psi event. First, the pulse height from each block was scaled to correspond to the amount of energy deposited during the

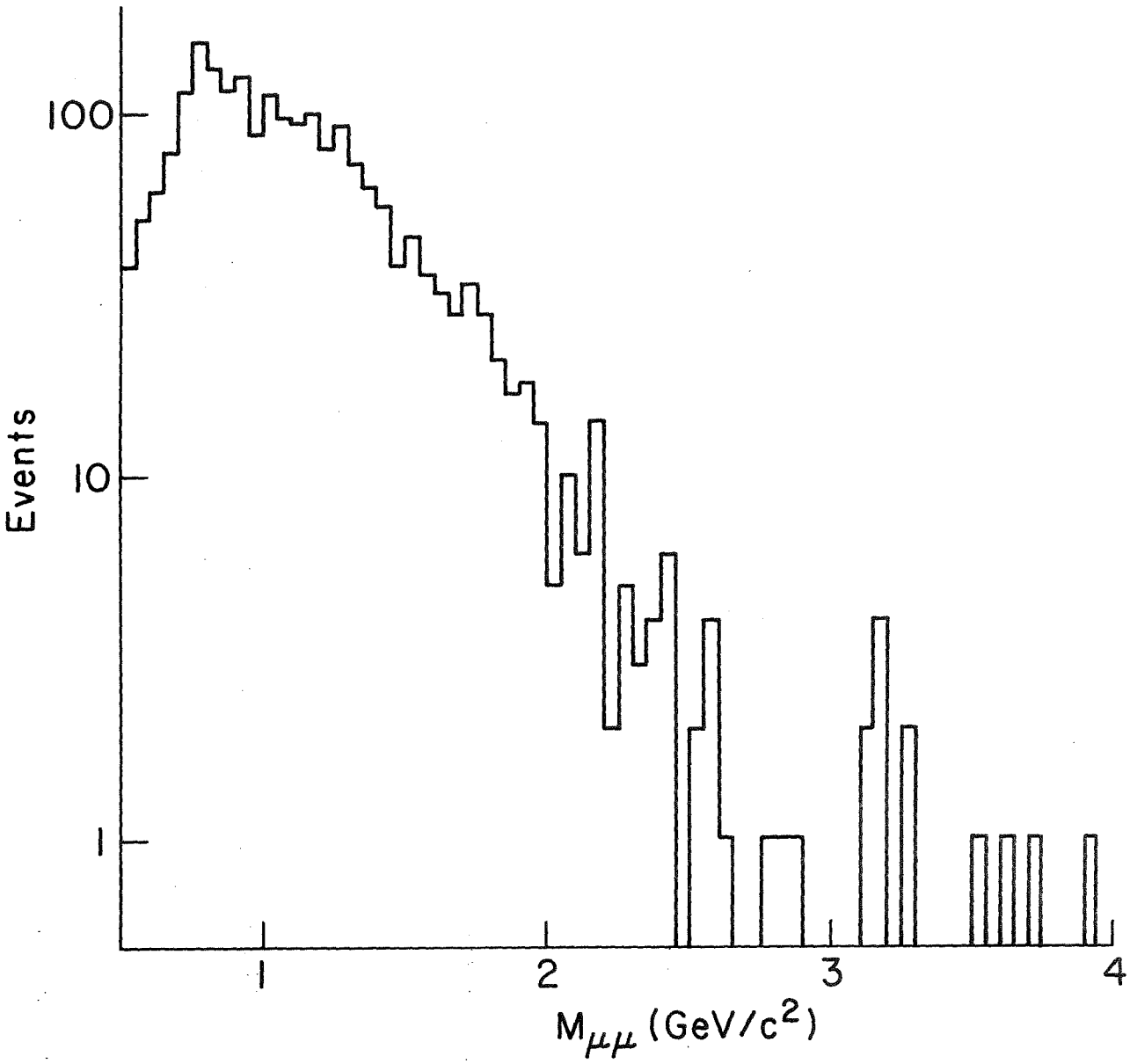

Figure 4-1. Early dimuon mass spectrum.

event. This procedure was fairly difficult since the calibration was not a constant but changed due to yellowing of the glass from radiation damage as the experiment progressed. There was also a baseline shift in the photomultiplier tubes for the lead glass which was correlated with instantaneous beam intensity. In order to compensate for the yellowing, the standard pulses fed to the lead glass at the beginning of each run were used. In addition, the gains were adjusted using an iterative procedure based on minimizing the reconstructed width of the neutral pion. Beam intensity was monitored for the hundred events prior to an event of interest to calculate the correction for baseline shift. The pi-zero peak with and without background subtraction is shown in Figures 4-2,3. The background was determined by combining uncorrelated photons and then normalizing to equal numbers of events for signal and background in the mass region 250-500 Mev/c .

Whenever a charged particle hit the lead glass, chances were high that it would interact. For the psi events, there were an average of 0.96 in-time charged particles striking the lead glass each event, with a maximum of 8 particles. This could easily lead to trouble since the hadronic shower resulting from an interacting particle spreads quite erratically as it develops in the lead glass and thus cannot be easily eliminated using a knowledge of the position of the incoming track. To remove these hadrons, and also to remove those

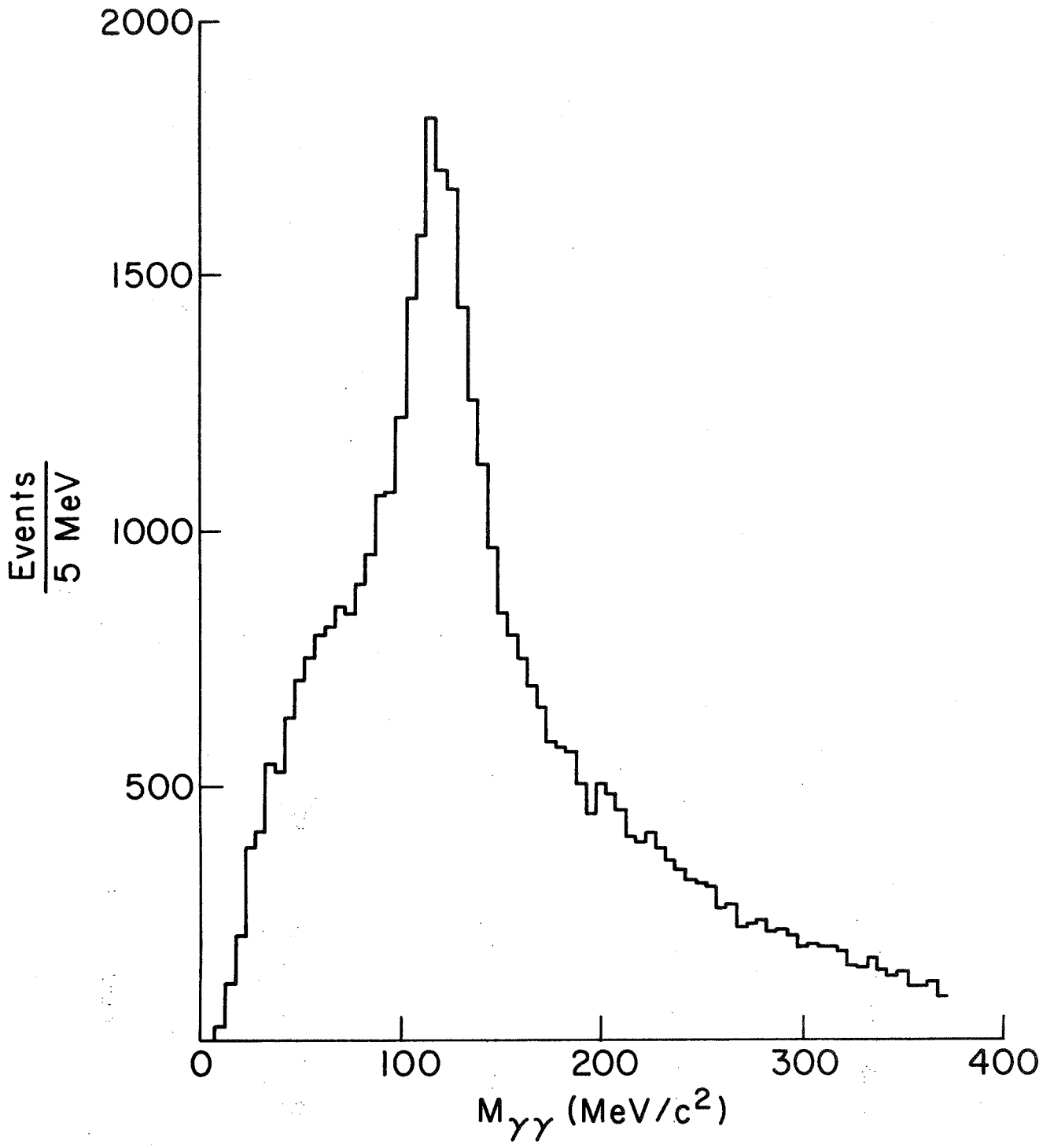

Figure 4-2. Diphoton mass spectrum.

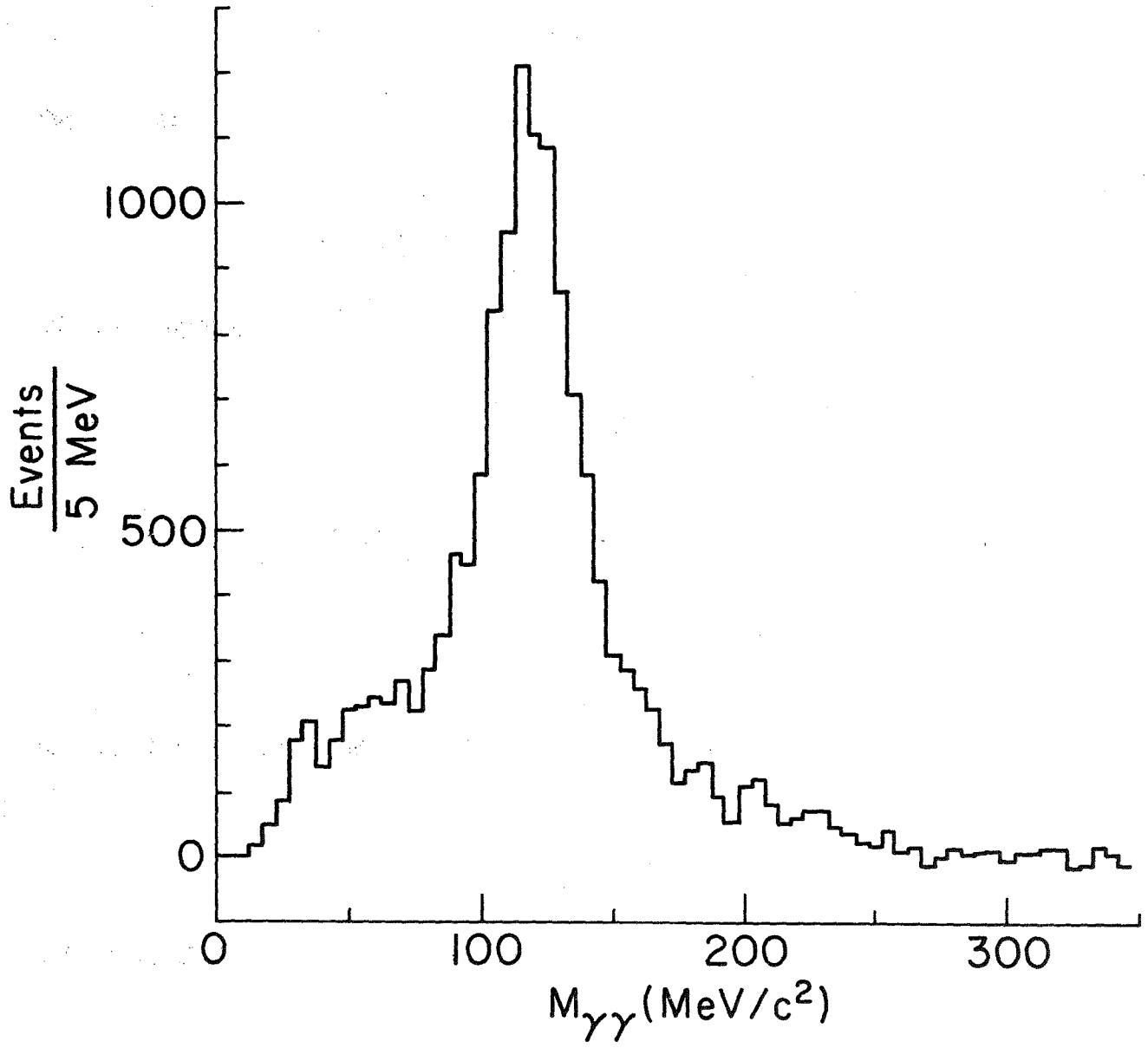

Figure 4-3. Diphoton mass spectrum with background subtracted.

showers so badly reconstucted as to be unreliable, a quality factor was calculated for each shower. This factor, Q, was defined as

$$Q = \frac{\#\text{ blocks in shower} - 3}{\sum_{i=1}^{3} E_i/E_{tot}} + 100 \sum_{4}^{6} E_i/E_{tot} \qquad (1)$$

where E_i is the energy deposited in block i, with the blocks arranged in order of decreasing energy, and all showers are defined to be contained within a 3x3 array of blocks. This test was designed using data gathered after the experiment during a calibration run using a monochromatic electron beam. See Figure 4-4 for the response of a typical block. Since an ideal shower would be contained in about three to four blocks, a good shower implies a low Q factor. A hadronic shower, which tends to be incredibly sloppy, will produce a large Q. In Figures 4-5a and 4-5b we see a plot of Q for the electron calibration, with either 75-100% of the shower energy deposited in the center block, or 50-75%. It is easily seen that the vast majority of showers have a Q below the cut value of 10. For the 75-100% signal, 98% have a Q factor between 0 and 10. Q for showers associated with hadrons is shown in Figure 4-5c. Figure 4-6 shows the number of pi-zeros reconstructed when a given upper limit for Q is imposed on the photons.

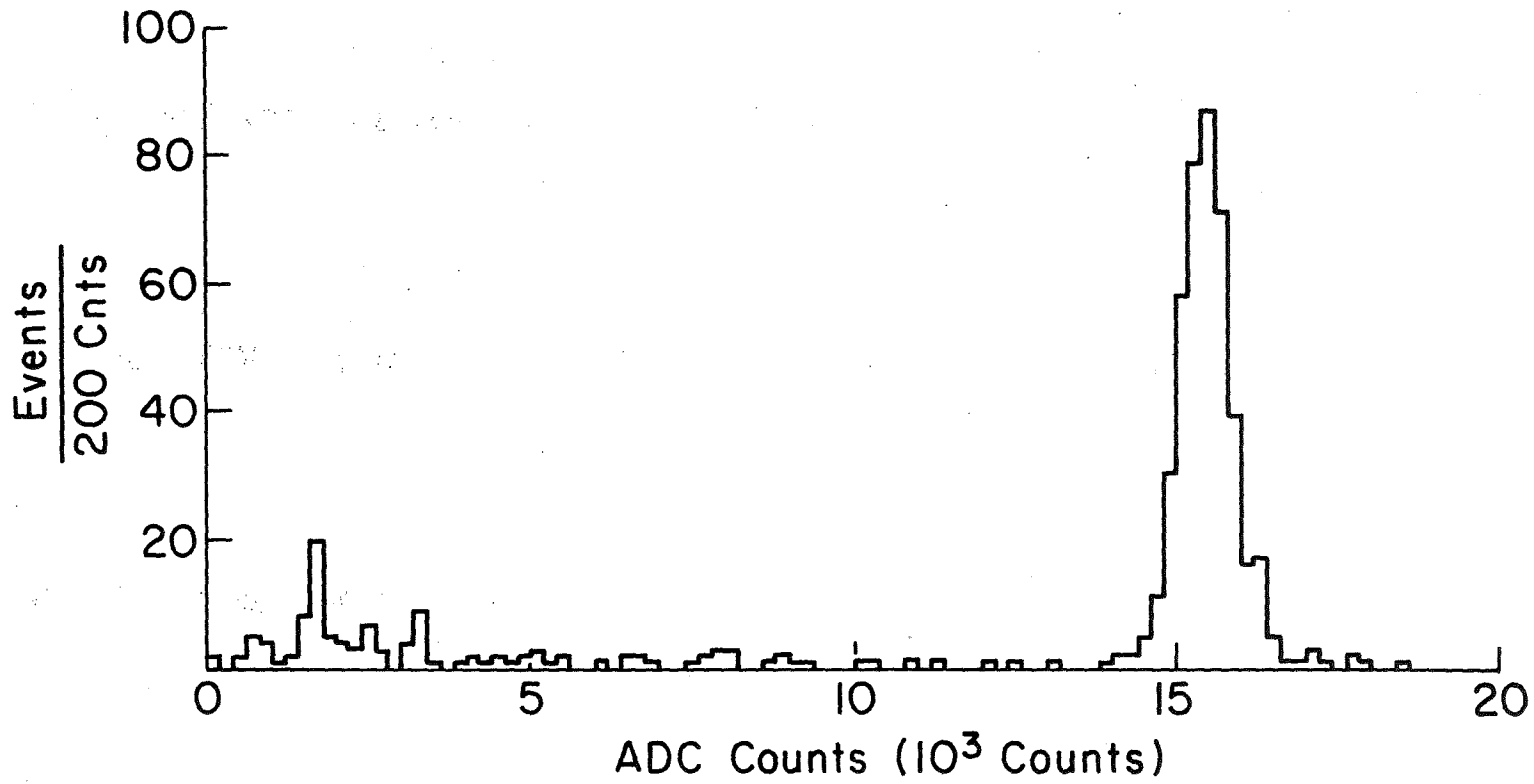

Figure 4-4. Response curve for a typical lead glass block during e^- calibration run.

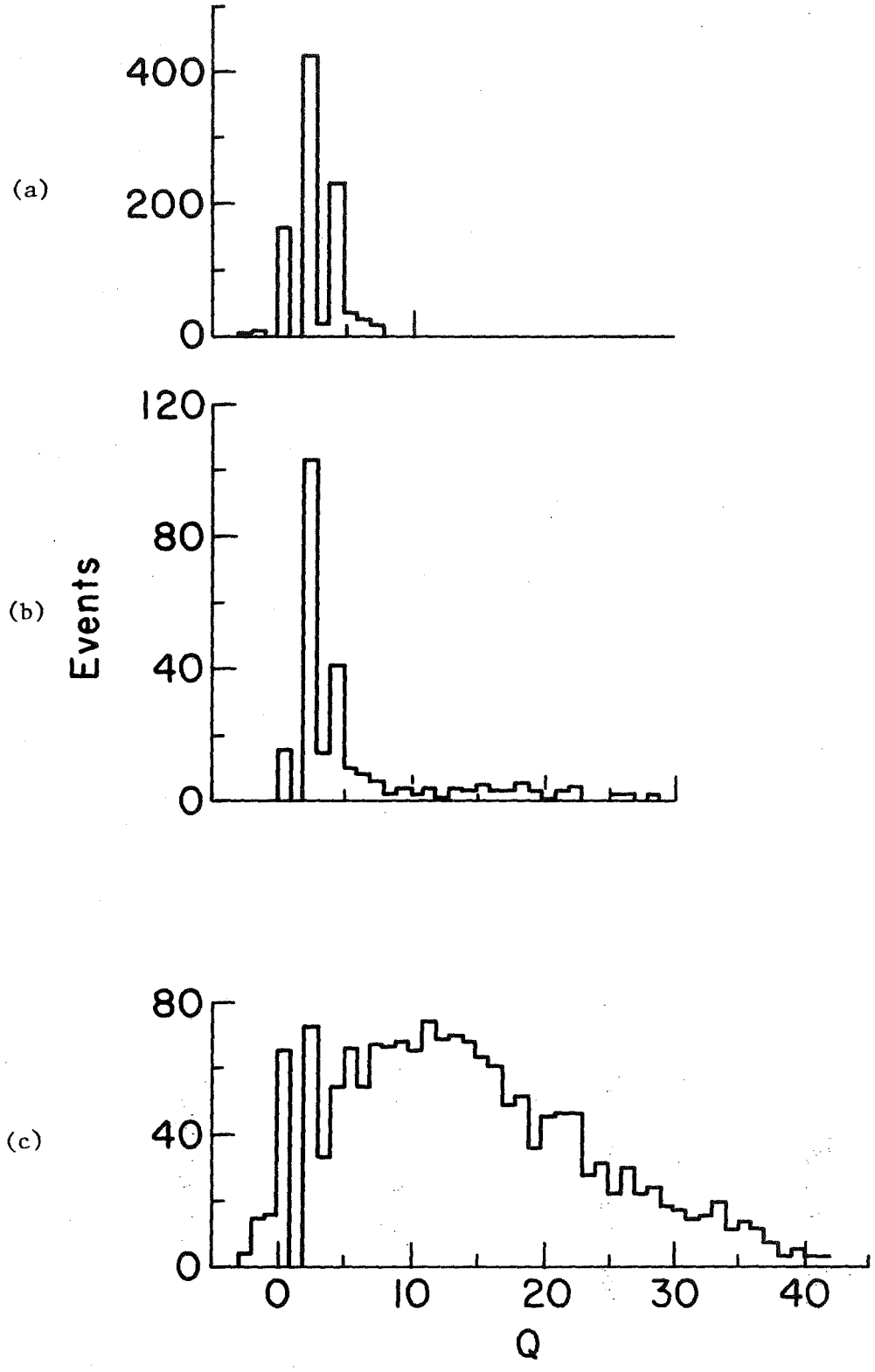

Figure 4-5. Quality factor.
(a) 75-100% of E_{tot} in center block,
(b) 50-75%,
(c) hadronic showers.

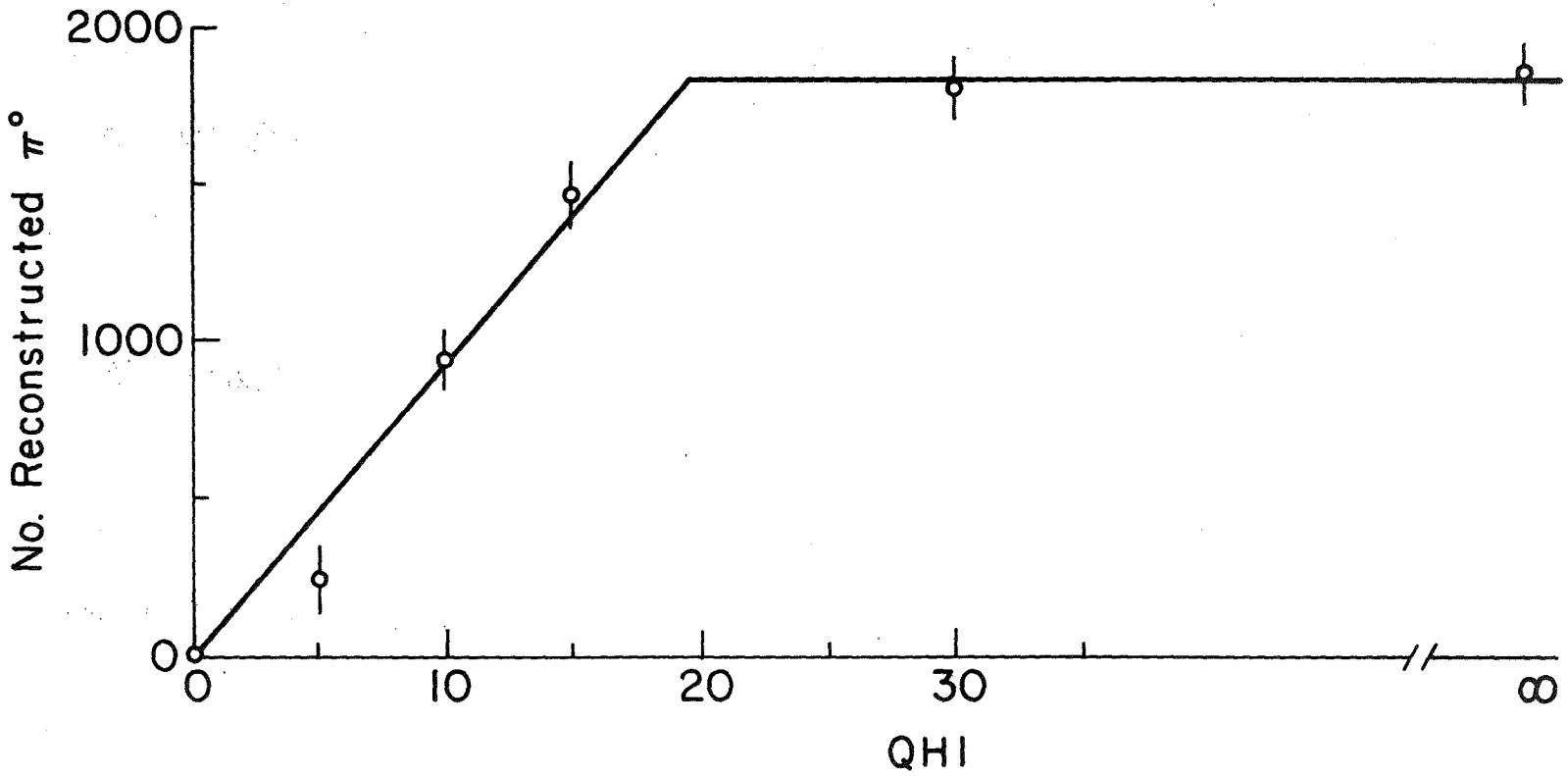

Figure 4-6. Number of reconstructed π° as a function of Q upper limit.

CHAPTER 5.

RESULTS

The calculation for the acceptance of our apparatus was done using a straightforward Monte Carlo approach. We assumed some dependence on x-Feynman and p_T for a particle with the mass of the psi (or chi) and then used a computer to simulate various decay channels of interest, normally with the decay products at each stage having distributions determined only by phase space. The final decay products are then propagated through our simulated apparatus to see if they would finally have been detected. Comparison of the original distributions of events with those detected allows one to correct for biases introduced by the equipment. This method has the disadvantage of being dependent upon the original distribution chosen, but it also has the rather distinct advantage of being the only system usable with a system of the complexity of the Muon Lab.

For the decay $\psi \rightarrow \mu\mu$, the parent distribution comes from the measurements made by Branson et. al.[1] on the reaction $\pi^- C \rightarrow \mu\mu + X$. These measurements were also made at the Muon Lab, albeit with a different configuration than the one we used. The actual

parametrization used for our calculation was

$$\frac{d^2\sigma}{dx_F dp_T} = \frac{1}{E_{\psi_{cm}}} \left(1 - x_F\right)^{2.0} e^{-2.2p_T} \quad . \qquad (1)$$

Not having any similar data available for chi production, we assumed the same distribution for this process as for psi production. That is, we produced the chis at whichever mass was of interest (the 3.45 Gev, 3.51 Gev, or 3.55 Gev chi state) according to Equation 1, and then let them decay isotropically in the chi rest frame into a psi and a photon. the resulting psi would then decay isotropically in its rest frame to produce two muons which might be detected. What was actually generated, of course, was the four momenta of the muons. To convert them into the analog of a physical particle with track parameters in the form of intercepts and slopes relative to the CCM, an interaction vertex was picked which was either in the beryllium or the hydrogen target with equal probability. Those vertices in the hydrogen were randomly distributed along the length of the target. The track parameters of the particles were changed to allow for the bend acquired by passing through the CCM. A field map was available for the magnet, but we used a simple hard-edged field approximation. The track parameters were again modified because of the multiple Coulomb scattering which would occur in the lead wall and steel hadron

absorber lying between the magnet and the final P-hodoscope detector. The deviation between unscattered and scattered tracks was determined by picking a set of random numbers in such a manner that they formed a Gaussian distribution with a standard deviation given by the standard formula for multiple scattering [2] for a particle of the given momentum. We then knew the x-y position of the muons at the P-hodoscope, and using the actual surveyed positions of its elements, we could determine if that particular event would have been detected. To check for detection of the photon coming from a chi decay, we additionally required that the photon track parameter should intersect the lead glass array.

The acceptance curves for the detection of the psi are shown in Figure 5-1,5-2, 5-3, and 5-4. In Figure 5-1a we have the distribution of psis in x_F as originally generated. Figure 5-1b shows those psis which would have been detected by the apparatus, and Figure 5-1c displays the ratio of Figure 5-1b to Figure 5-1a. Because low momentum particles fail to pass through the magnet, the acceptance is highest in the high x_F region, where it approaches 50%. The overall acceptance, of the parent particle generating distribution we used was found to be 9.3%. Figure 5-2 is a similar set of graphs with p_T as the variable of interest. Figure 5-2a and Figure 5-2b show $(p_T)^{-1}(dN/dp_T)$ as a function of p_T, and Figure 5-2c is their ratio. A hand drawn line has been superimposed to guide the eye. Here we see a

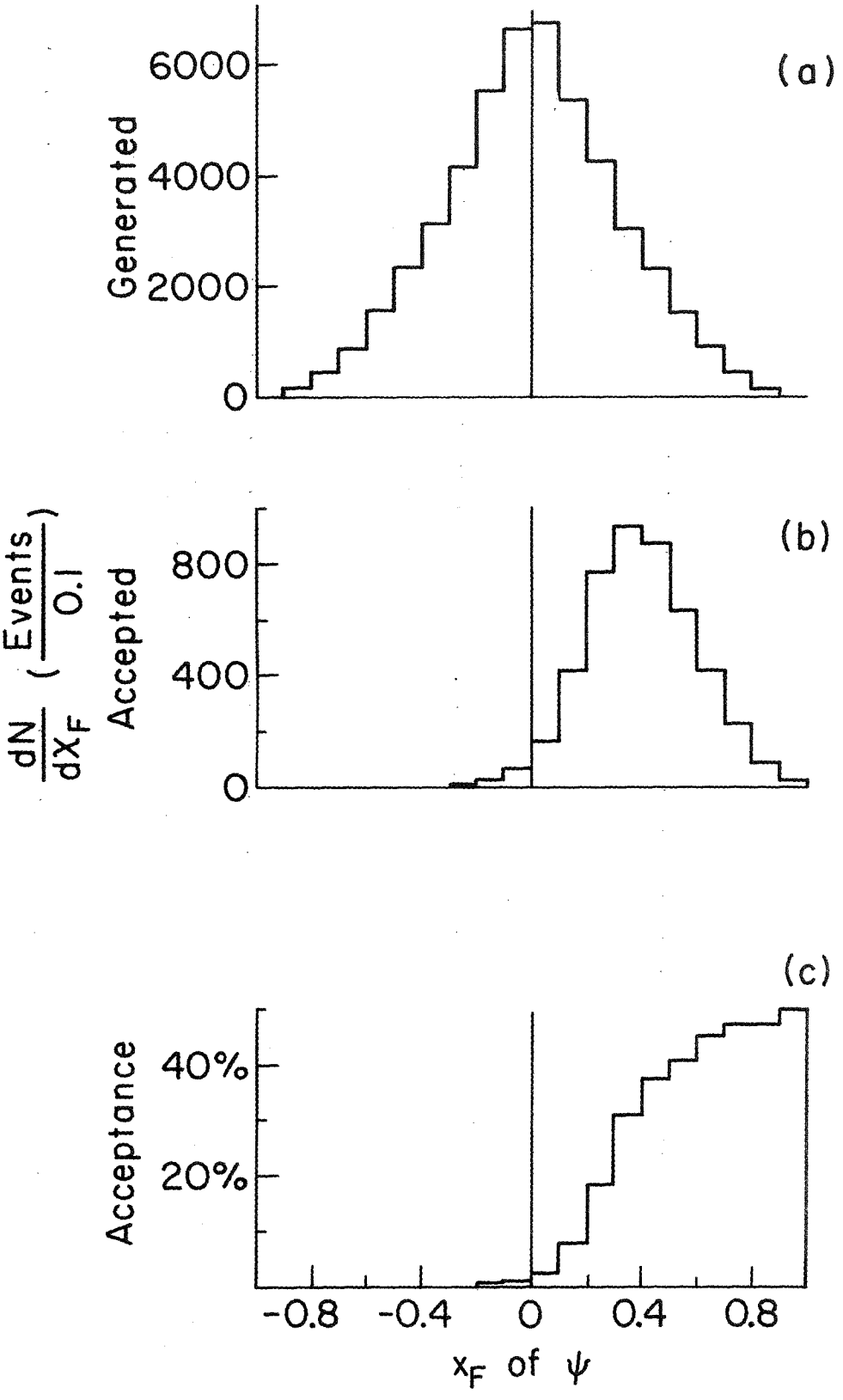

Figure 5-1. Acceptance of ψ events as a function of x_F.

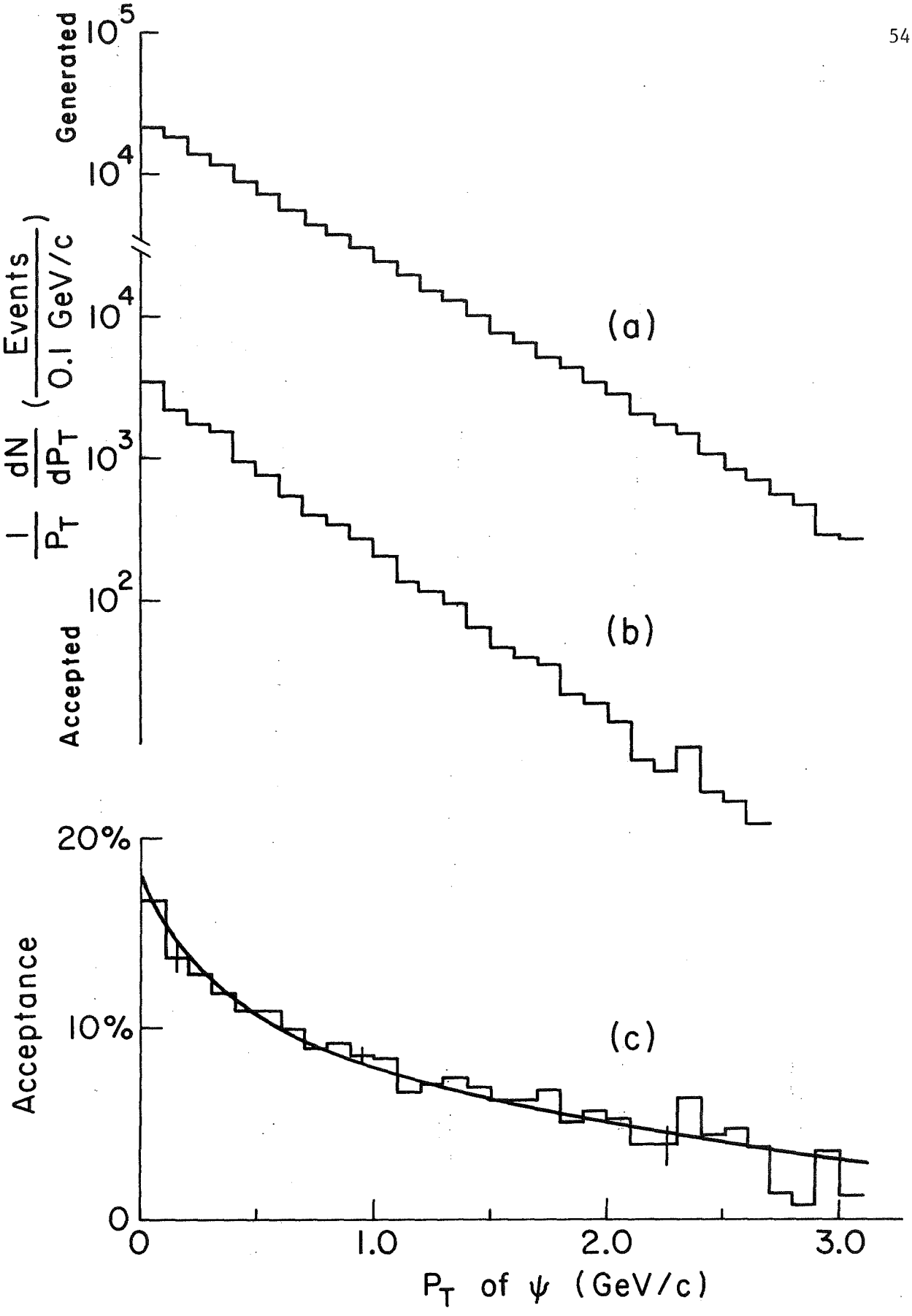

Figure 5-2. Acceptance of ψ events as a function of p_T.

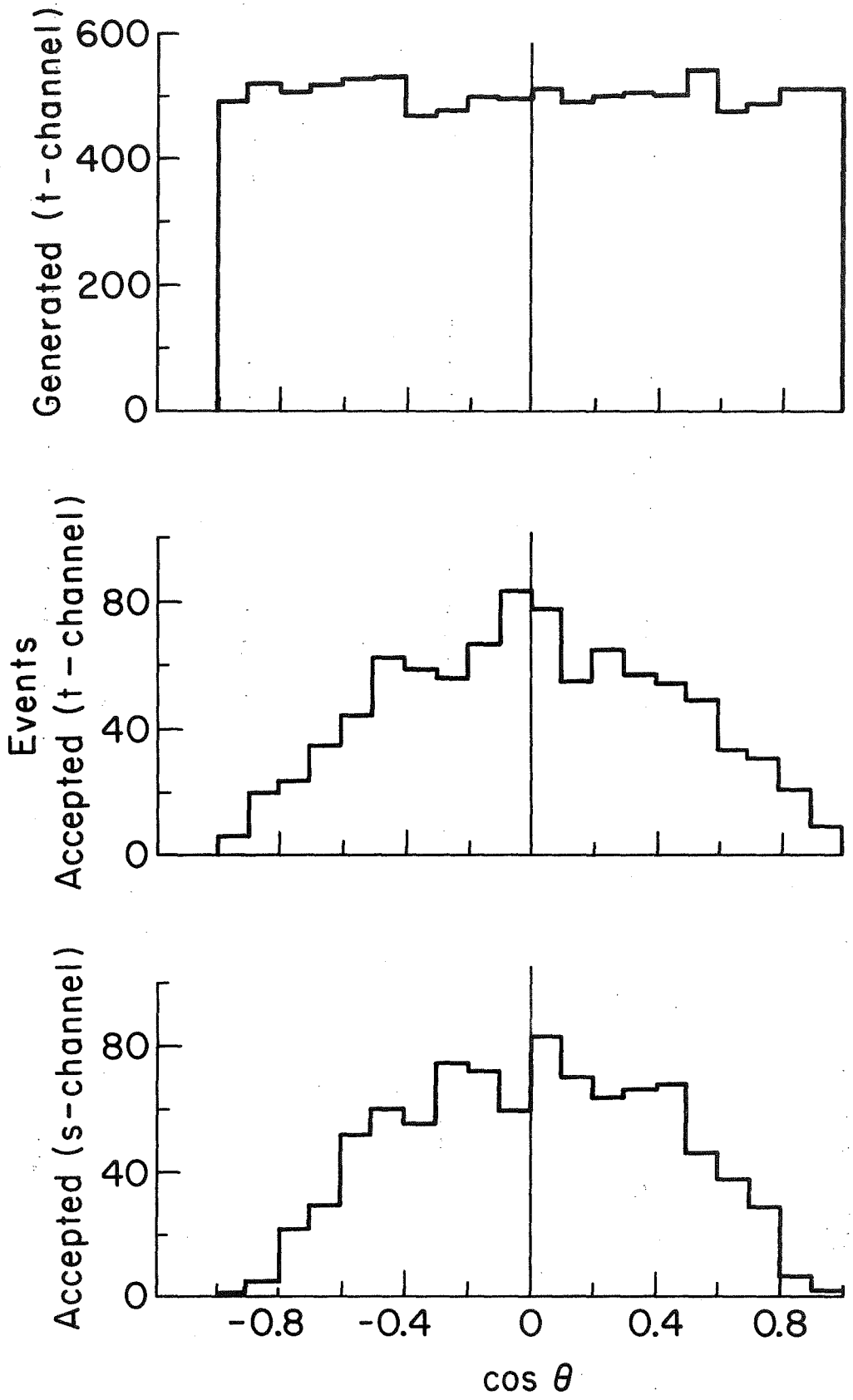

Figure 5-3. Acceptance of ψ events as a function of cosθ (generated flat).

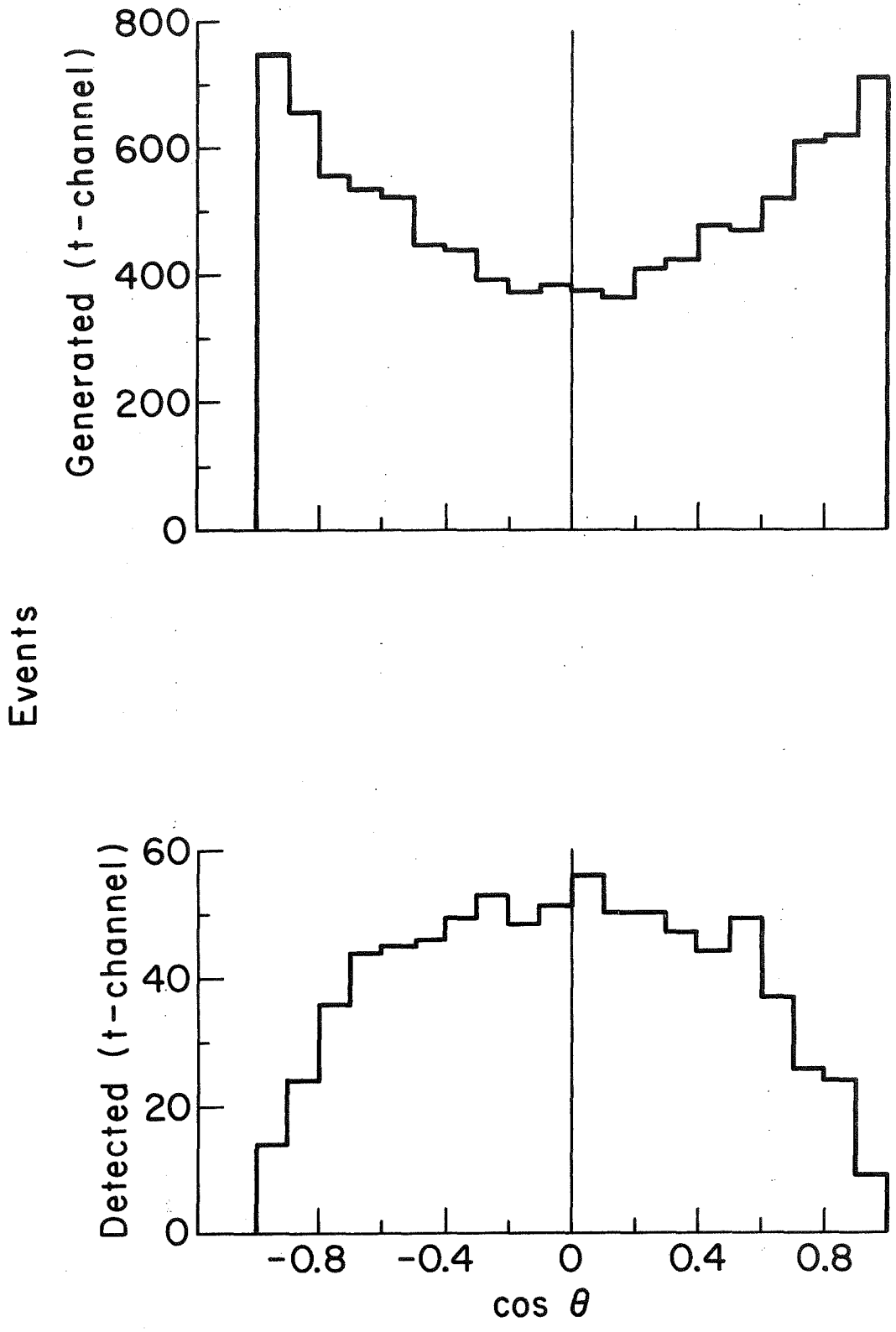

Figure 5-4. Acceptance of ψ events as a function of $\cos\theta$ (generated $\sim 1 + \cos^2\theta$).

gradual drop in acceptance with p_T ,as the daughter muons tend to either hit the pole faces of the CCM or miss the edges of the P-hodoscope.

The angular dependence of the muons (and the gamma for chis) can be very interesting since QCD makes very definite predicitions here (see [3] and [4]) but it is apparent from Figures 5-3 and 5-4 that any correlation would be very difficult for us to see. These figures show the distribution for the angle between the positive muon and either the incident beam particle (t-channel) or -(recoil system direction) (s-channel), with the calculation done in the rest frame of the psi. In Figure 5-3a is the distribution of $\cos\theta$ (t-channel) generated with no theta dependence and Figures 5-3b and 5-3c show the distribution of detected events plotted in either the t or s channel. Figure 5-4a is the distribution of the $\cos\theta$ (t-channel) generating function of $1+\cos^2\theta$ (t-channel). This was taken as the extreme case where differences in angular dependence would be most apparent. Figure 5-4b is the distribution of the accepted events. It is all too clear that due to the small acceptance for $|\cos\theta|\sim 1$ a very large sample would be necessary before a statistically significant determination could be made.

The results of similar acceptance calculations in x_F and p_T are shown in Figures 5-5 and 5-6 using a parent particle mass of 3.42 Gev. The constraints imposed by the apparatus are again reflected in the

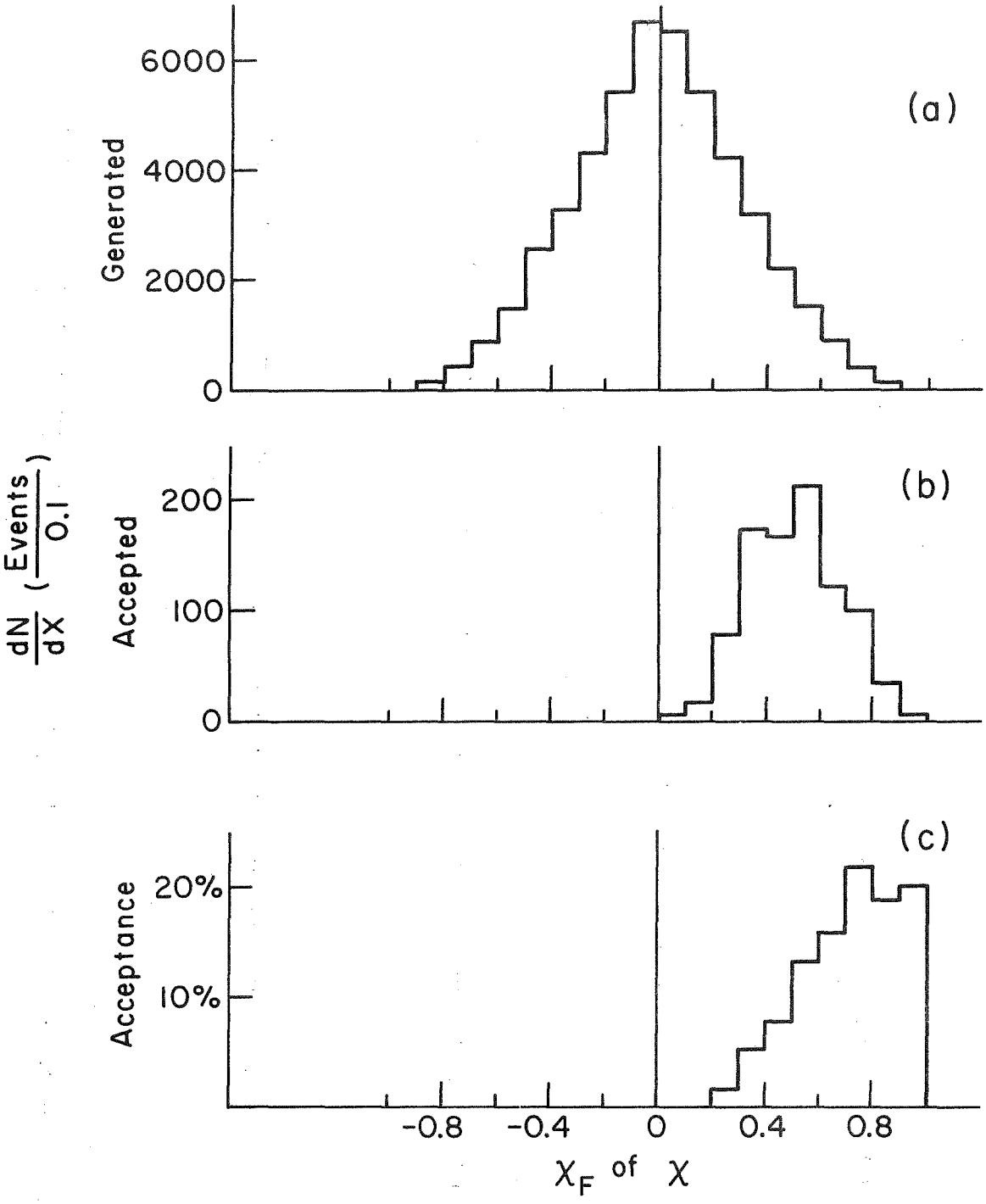

Figure 5-5. Acceptance of χ events as a function of x_F.

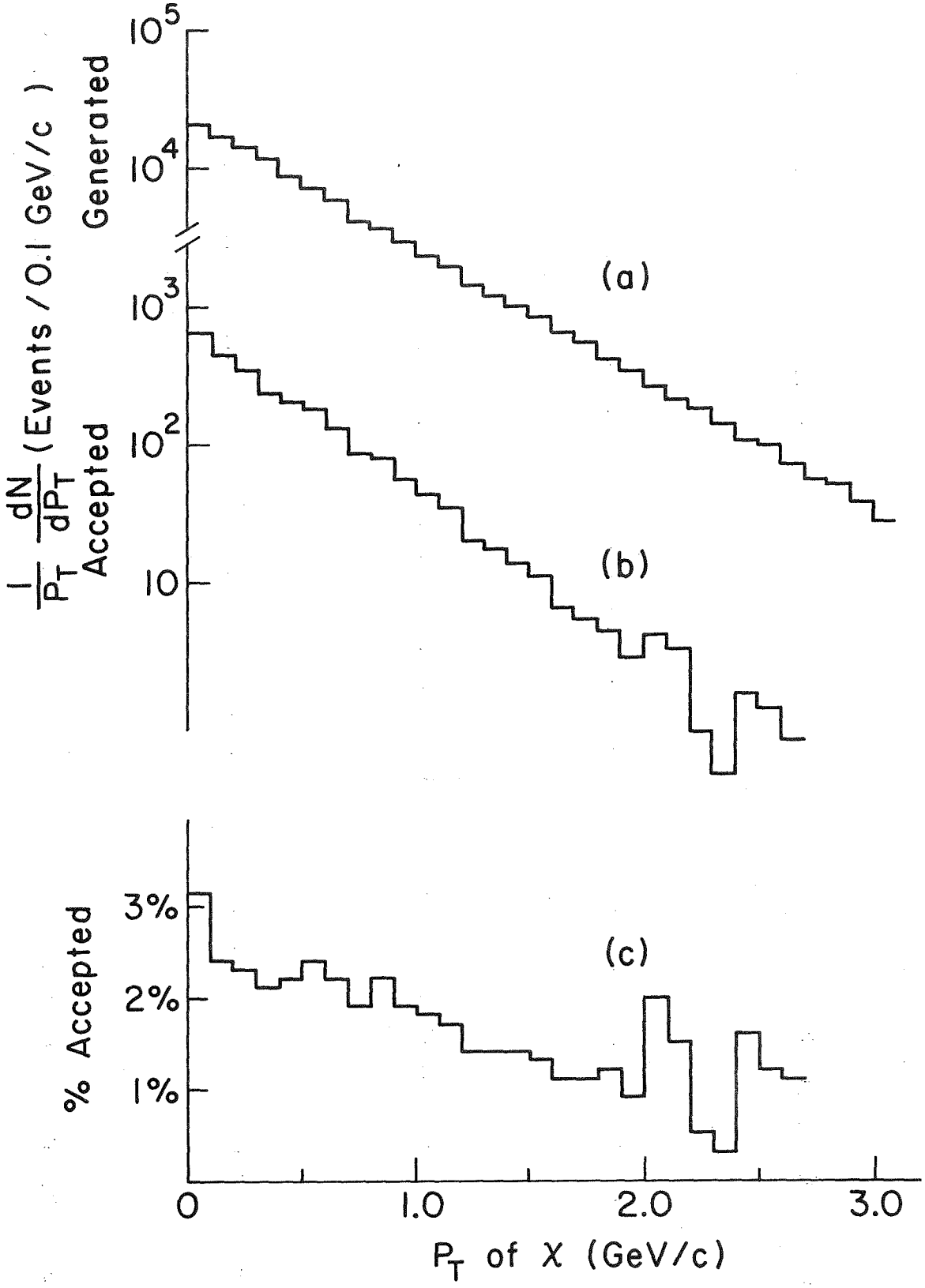

Figure 5-6. Acceptance of χ events as a function of p_T.

acceptance, but the photon requirement is now included. The distribution of photon energy before any equipment constraints is displayed in Figure 5-7a. The distribution after all constraints is shown in Figure 5-7b. The overall acceptance has dropped from 9.3% to 1.9%. For a particle mass of 3.55 Gev it is 1.7%.

Now that we have calculated the acceptance, we can examine the actual data. Figure 5-8a is the original psi sample, that is, the 234 events in the dimuon mass spectrum lying between 2.9 Gev and 3.3 Gev. Figure 5-8c shows the (one constraint) chi-squared distribution formed when fitting those events to a nominal mass of 3.098 Gev. Removing those events with a chi-squared greater than 10 from the distribution in Figure 5-8a results in the distribution shown in Figure 5-8b. We decided upon a chi-squared of 10 because this removes the number of events which we expect to find in the background in the region 2.9-3.3 Gev. We made this background estimate by examining the dimuon mass spectrum in the regions above and below the psi mass and extrapolating between them to get an average background figure. These events with a chi-squared less than 10 compose the psi sample that is used to calculate all distributions, including those of the chis. Figure 5-9 shows the beam momentum for the 216 events between 2.9 Gev and 3.3 Gev with a reconstructed beam track. Figure 5-9a is the distribution of beam momentum along the beam axis (pz) while Figures 5-9b and 5-9c are the x and y momentum distributions respectively. In Figures 5-10a,b,

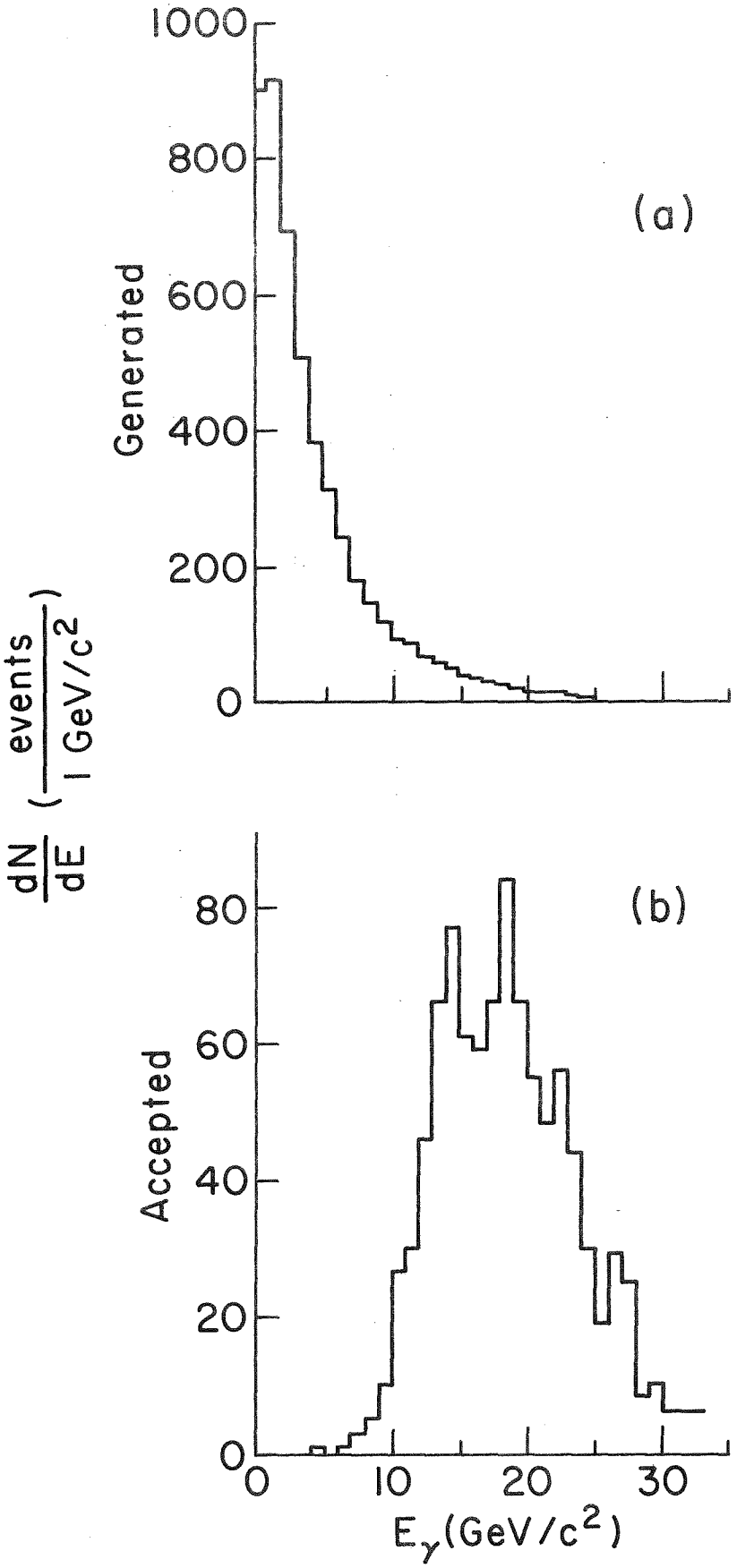

Figure 5-7. Acceptance of χ events as a function of E_γ.

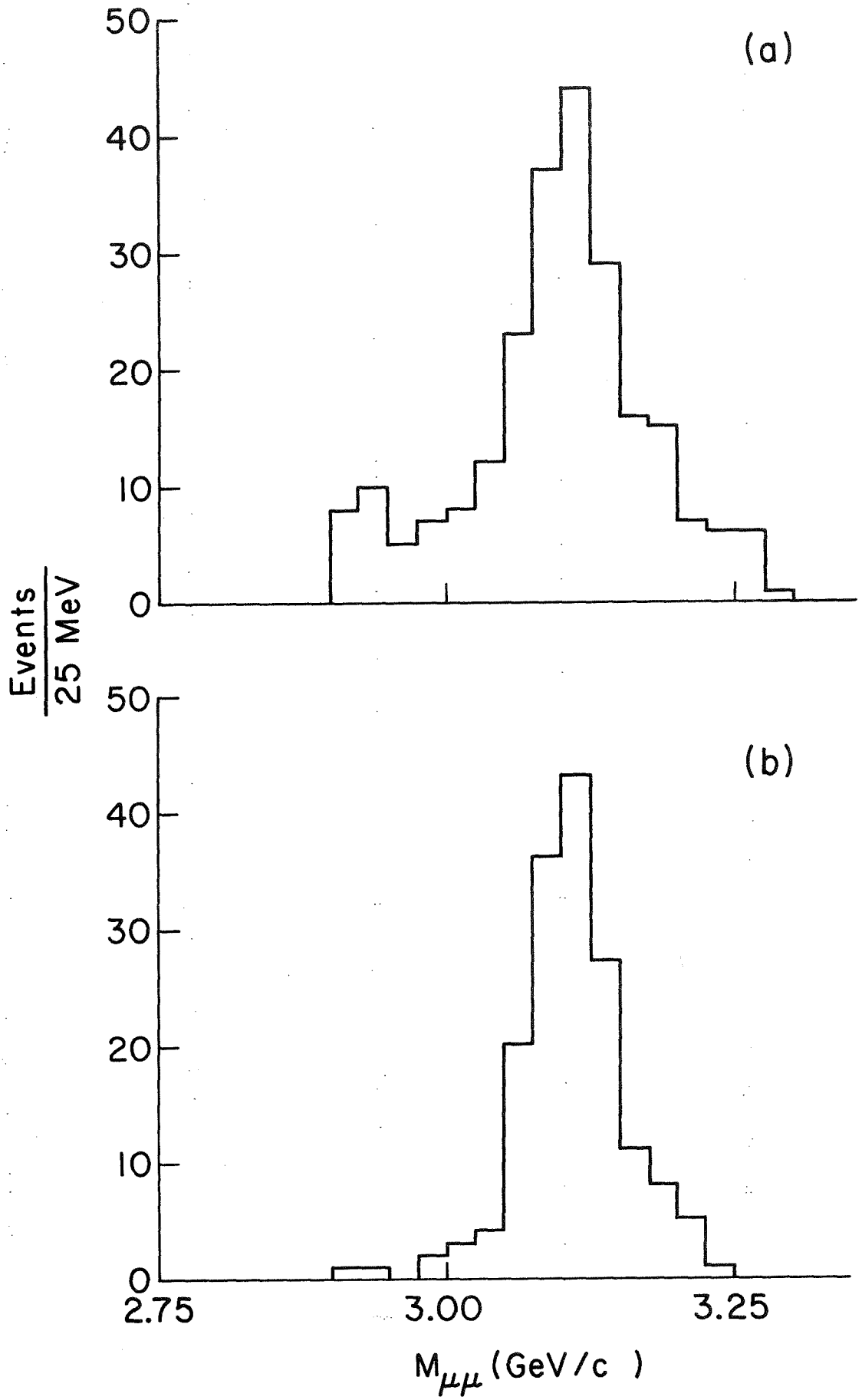
(a)
(b)
50
40
30
20
10
0
Events / 25 MeV
2.75
3.00
3.25
$M_{\mu\mu}$ (GeV/c)

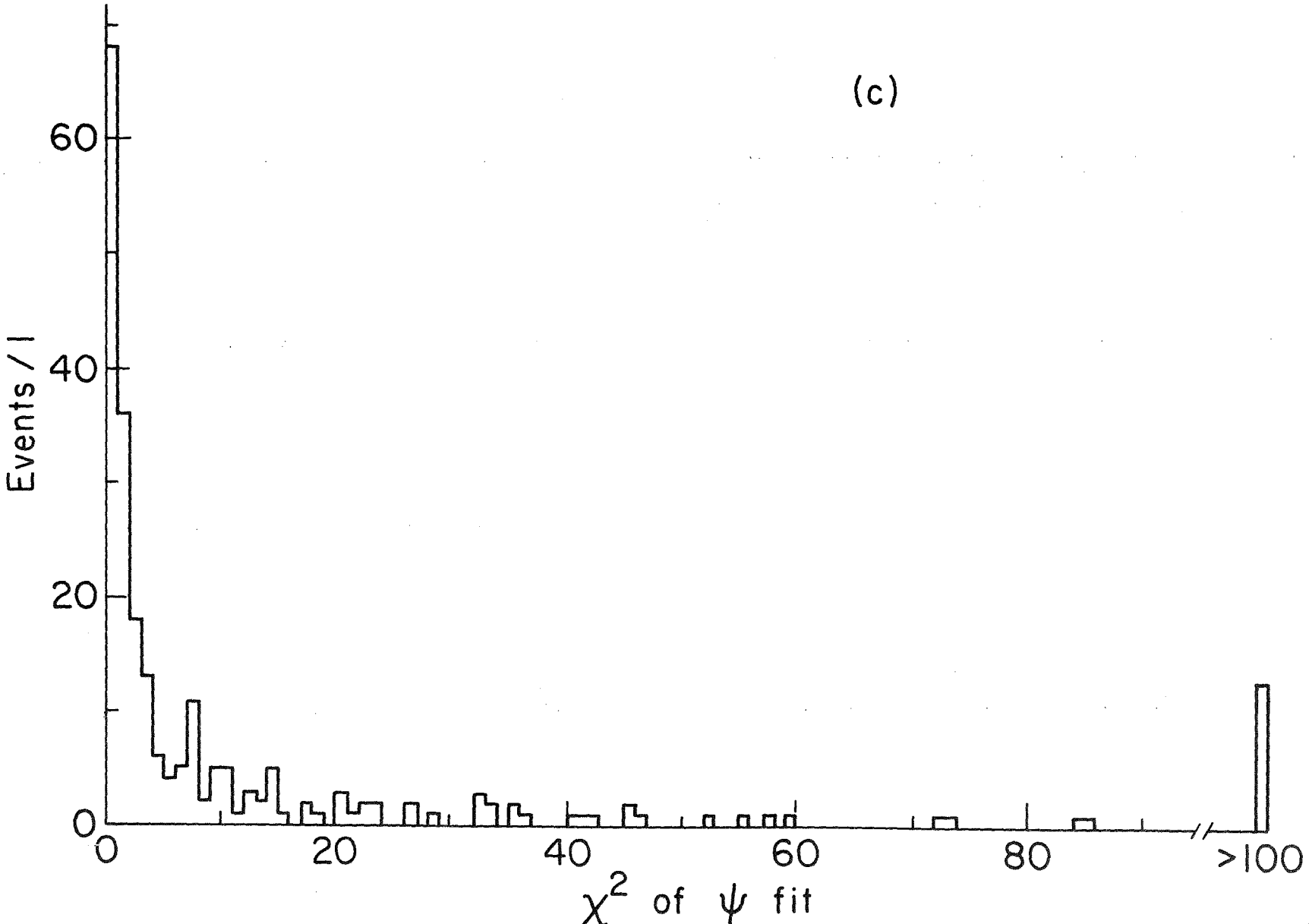

Figure 5-8. The ψ signal.
(c) χ^2 for 1 constraint hypothesis.

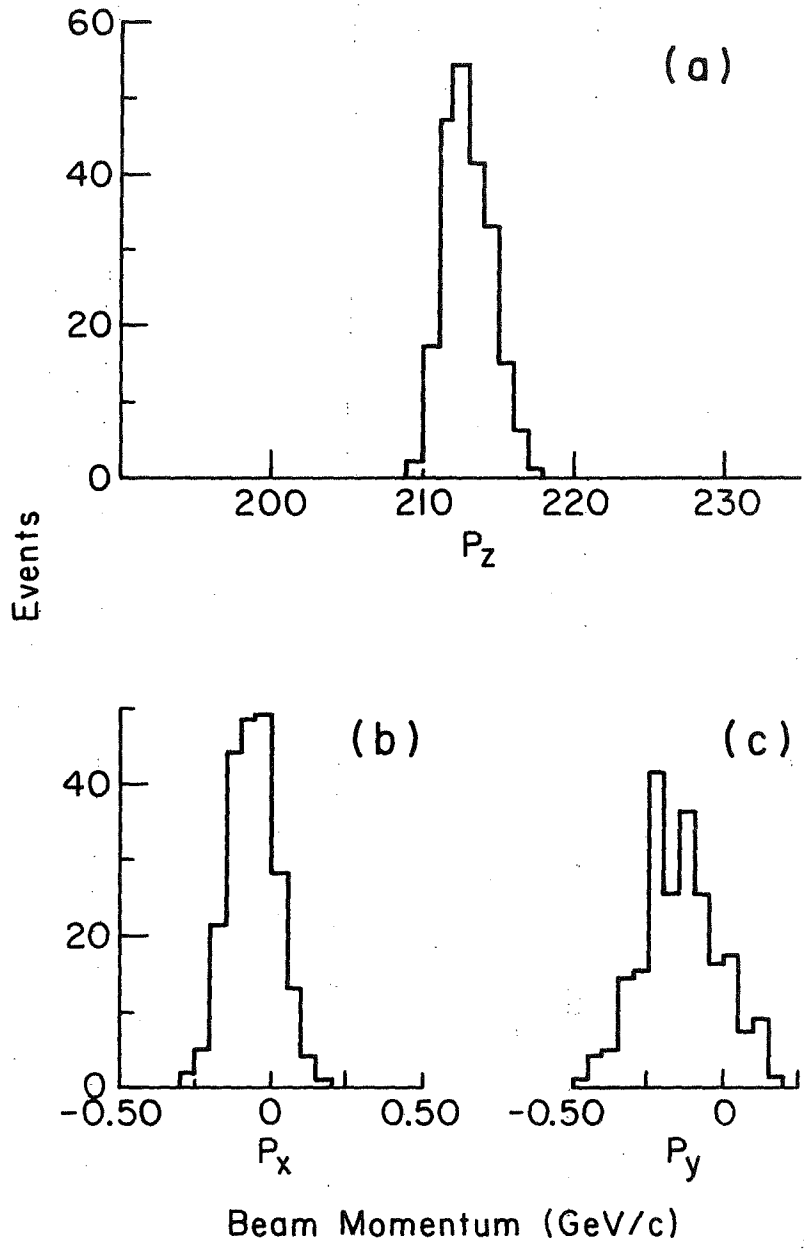
60
40
20
0
(a)
200
210
220
230
P_z
Events
(b)
(c)
40
20
0
-0.50
0
0.50
P_x
-0.50
0
P_y
Beam Momentum (GeV/c)

Figure 5-9.

and c, we have the distributions of the calculated vertex positions in x,y, and z for the psi sample. Figures 5-11a and 5-11b show the vertex position distributions for events classified by the target scintillators as occurring in either the beryllium or the LH2. We see that this classification scheme cannot be exact since there are events classified as "Be" which have their vertices far from the beryllium target. To remove these possibly pathological events we require that Be events occur at a z(vertex)<(-3000 1/4 mm's) and that LH2 events occur with z(vertex)>(-3000 1/4 mm). Calculating the x_F and p_T of these good events relative to the beam if it has been found and relative to a nominal value of p(beam)=(0,0,215 Gev) if it was not, we find the raw distribution x_F given by the solid histogram in Figure 5-12. After correction for acceptance we have the open circle points in Figures 5-12 and 5-13, which have a best chi-squared fit curve superimposed. The distributions were fitted to

$$\frac{dN}{dx_F} \propto \frac{1}{E_{\psi_{cm}}} \left(1 - x_F\right)^a \tag{2}$$

and

$$\frac{1}{p_T}\frac{dN}{dp_T} \propto e^{-bp_T} \quad . \tag{3}$$

The paramters a and b for both LH2 and beryllium are presented in Table 5-1 along with similar fits for different experiments using iron

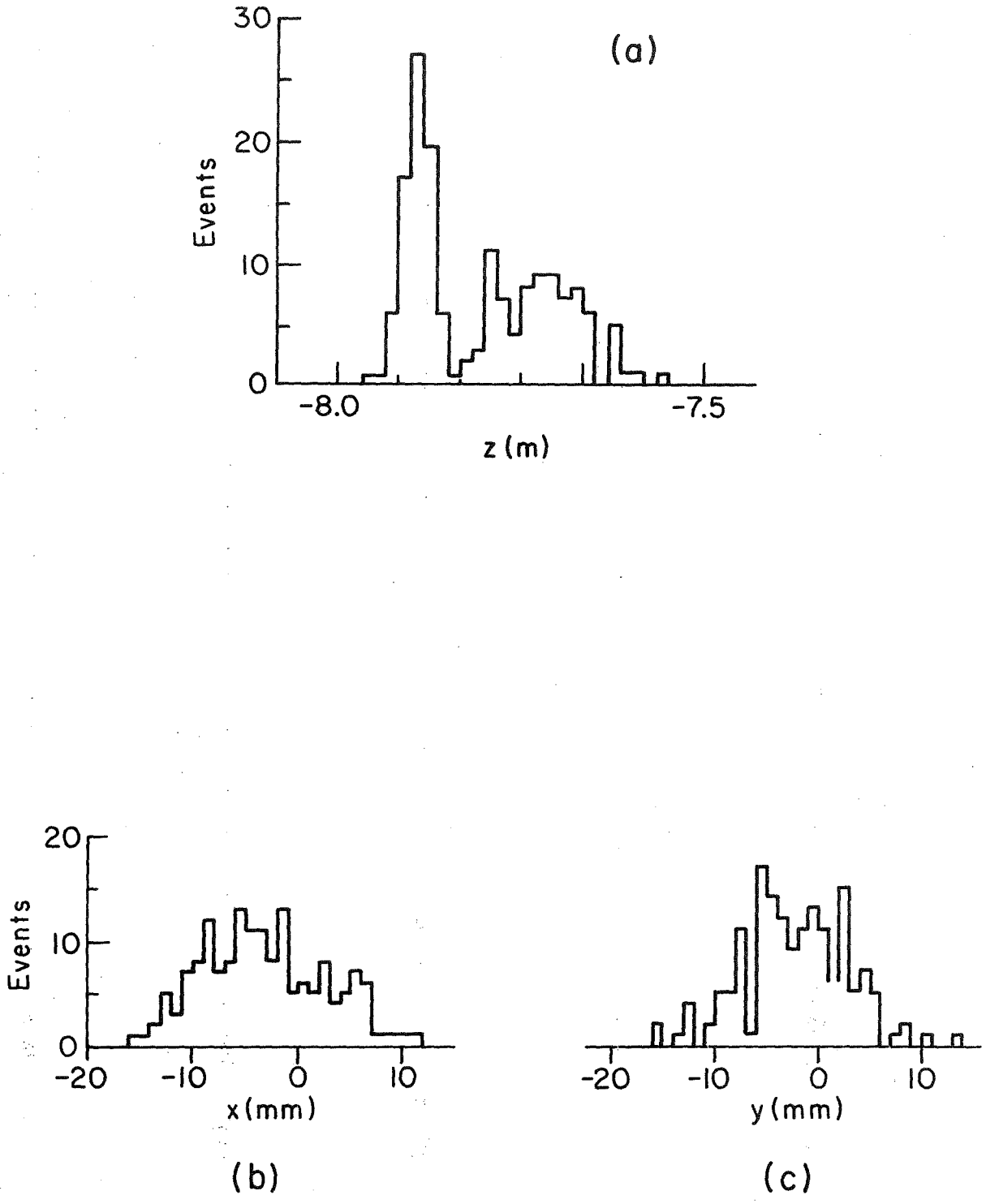

Figure 5-10. Vertex position for ψ events.

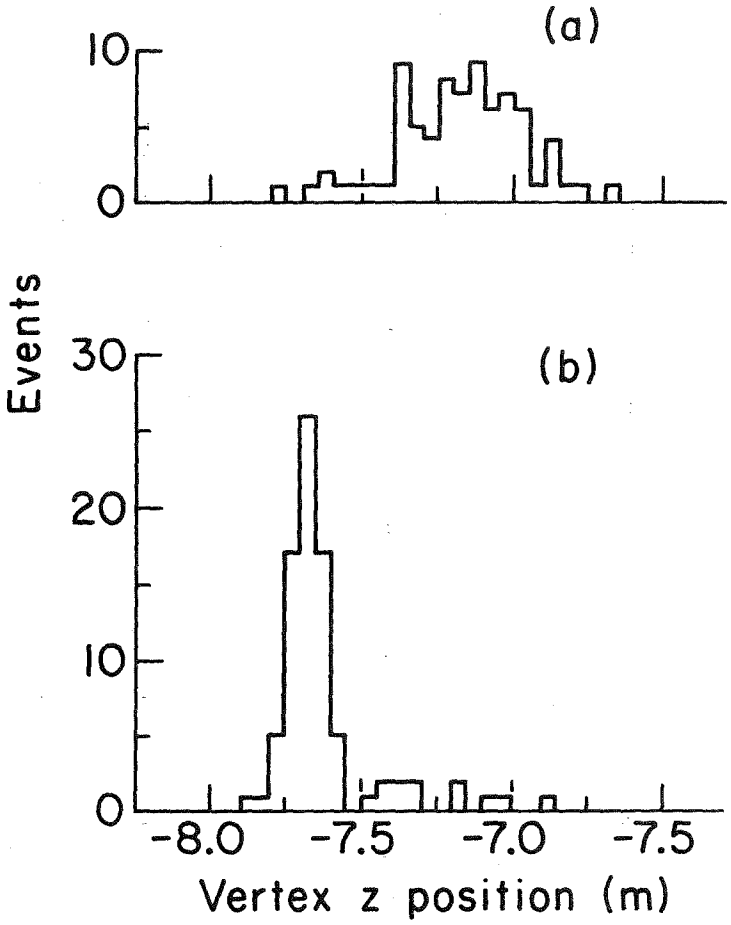

Figure 5-11. Vertex z position.
(a) for LH_2 events,
(b) for Be events.

Figure 5-12. x_F of ψ events.

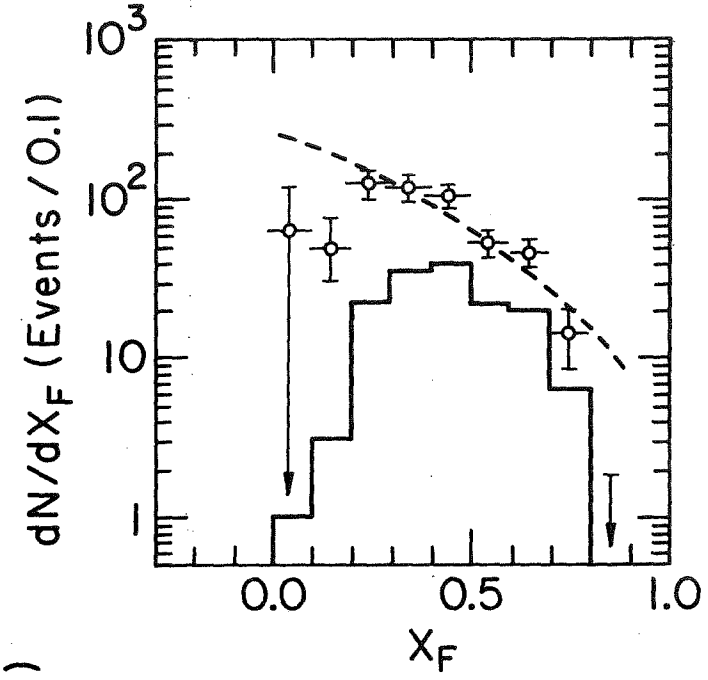

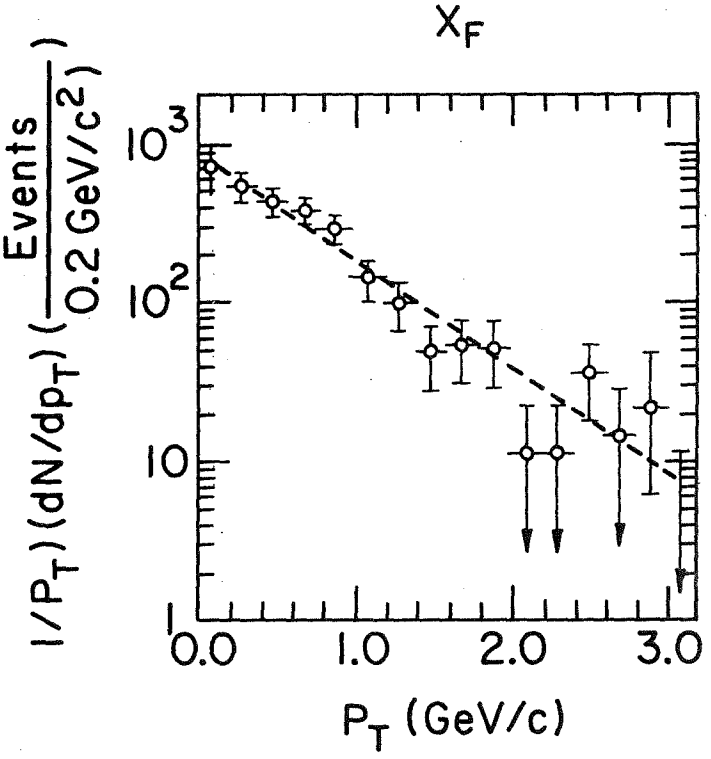

Figure 5-13. p_T of ψ events.

and carbon targets.

With the known interaction length of the LH2 target (3.5%), the acceptance for psis (9.3%), the total inelastic cross section for π^-p at 215 Gev (21.5 mb/nucleon), and the total number of pions on target during a 2_μ trigger run (2.7×10^{10}), we can make an estimate of the cross section for psi production. This is a rough estimate since we do not know the inefficiency of the track finder when searching for psis. Forging blindly ahead we determine from the 71 LH2 events that

$$\sigma B = 17 \text{ nb/nucleus} \tag{4}$$

or using the measured number B(branching ratio for psi$\rightarrow 2_\mu$)=7%

$$\sigma = 244 \text{ nb} \tag{5}$$

with a statistical uncertainty of 30 nb. If we knew the correct A(atomic number) dependence, this number could be compared with the result of B=141 +/- 10 nb for π^-C at 225 Gev which Branson [11] reports for $x_F>0$. To find our own A dependence, we compare our 72 Be events with the 71 LH2 events. Calculating the cross section per beryllium nucleus, we find

$$\sigma_{\text{nucleus}} = 0.646\ \sigma_{\text{LH2}} \quad . \tag{6}$$

Parametrizing this as

$$\sigma_{nucleus} = A^{\alpha}\ \sigma_{nucleon} \qquad (7)$$

we find $\alpha = .80 \pm 0.08$. This can be compared with Branson's value of $\alpha \sim 0.9$ [6] and Binkley's of $\alpha = .93 \pm .04$ for neutrons on Be, Al, Cu, and Pb [7]. Using Binkley's value we can unfold the 141 nb/nucleus to 28 ± 2 nb for σ_B.

Now that the subject of psis in and of themselves has been exhausted, we turn to the question of the particles produced in association with them. In Figures 5-14a and 5-15a we have x_F and p_T distributions for all found charged pions in psi events, with no acceptance corrections. Figures 5-14b and 5-15b show the same distributions for non-psi events (events away from the psi mass (2.5-2.9 Gev and 3.3-4.0 Gev) and chi-squared greater than 10 events in the psi region). Figures 5-16a and 5-16b show the charged particle multiplicity at the psi mass and in non-psi events. In Figures 5-17a and 5-17b we have the energy distributions (uncorrected) of photons found associated with the psis, graphed first on a linear scale and then on a semi-logarithmic scale. These photons have been required to have a quality factor, Q, such that $0<Q<10$, and an energy greater than 1 Gev. Also, all photons hitting the lead glass array near the beam region have been removed.

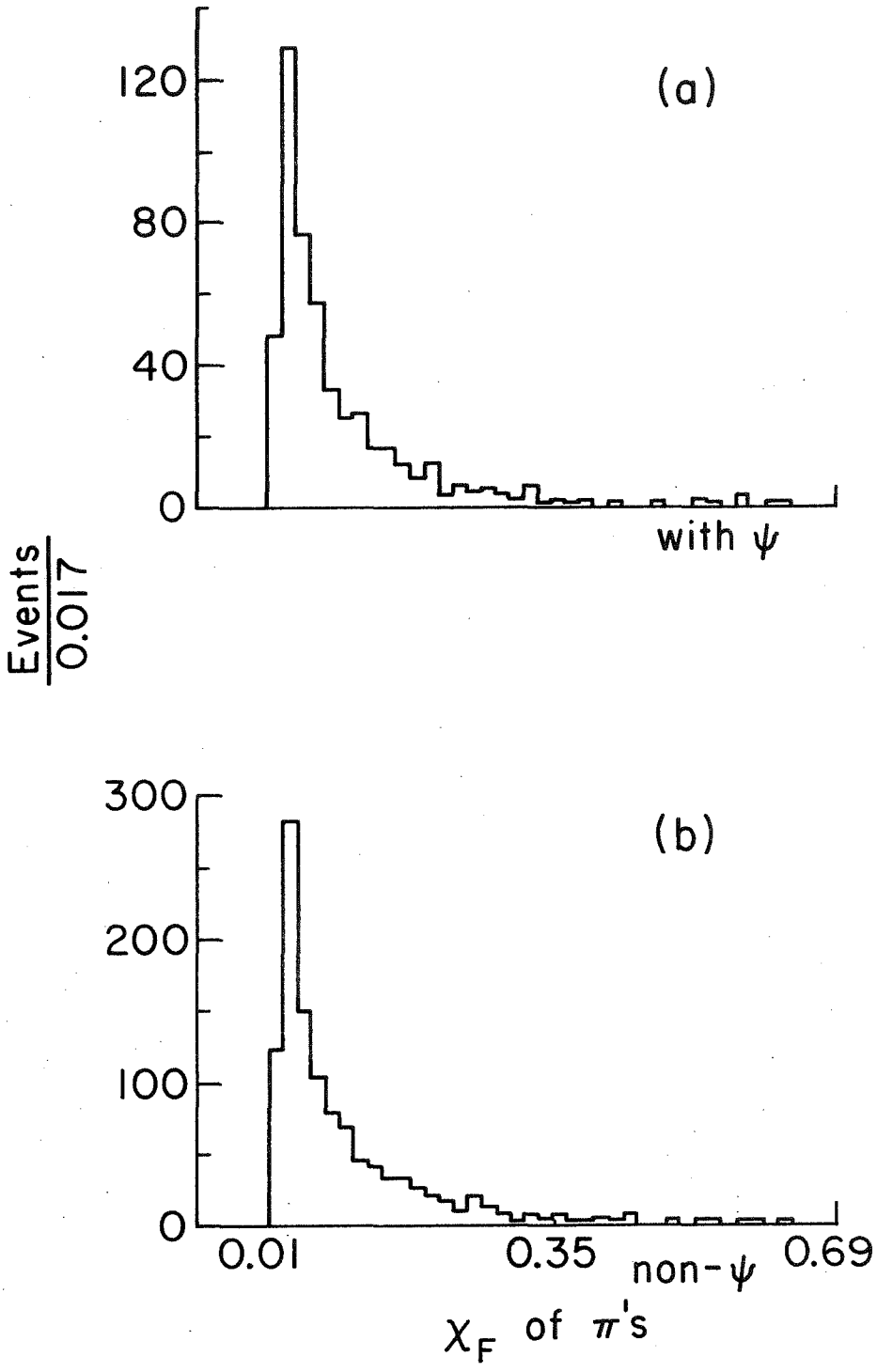
120
80
40
0
(a)
with ψ
Events / 0.017
300
200
100
0
(b)
0.01
0.35
non-ψ
0.69
X_F of π's

Figure 5-14.

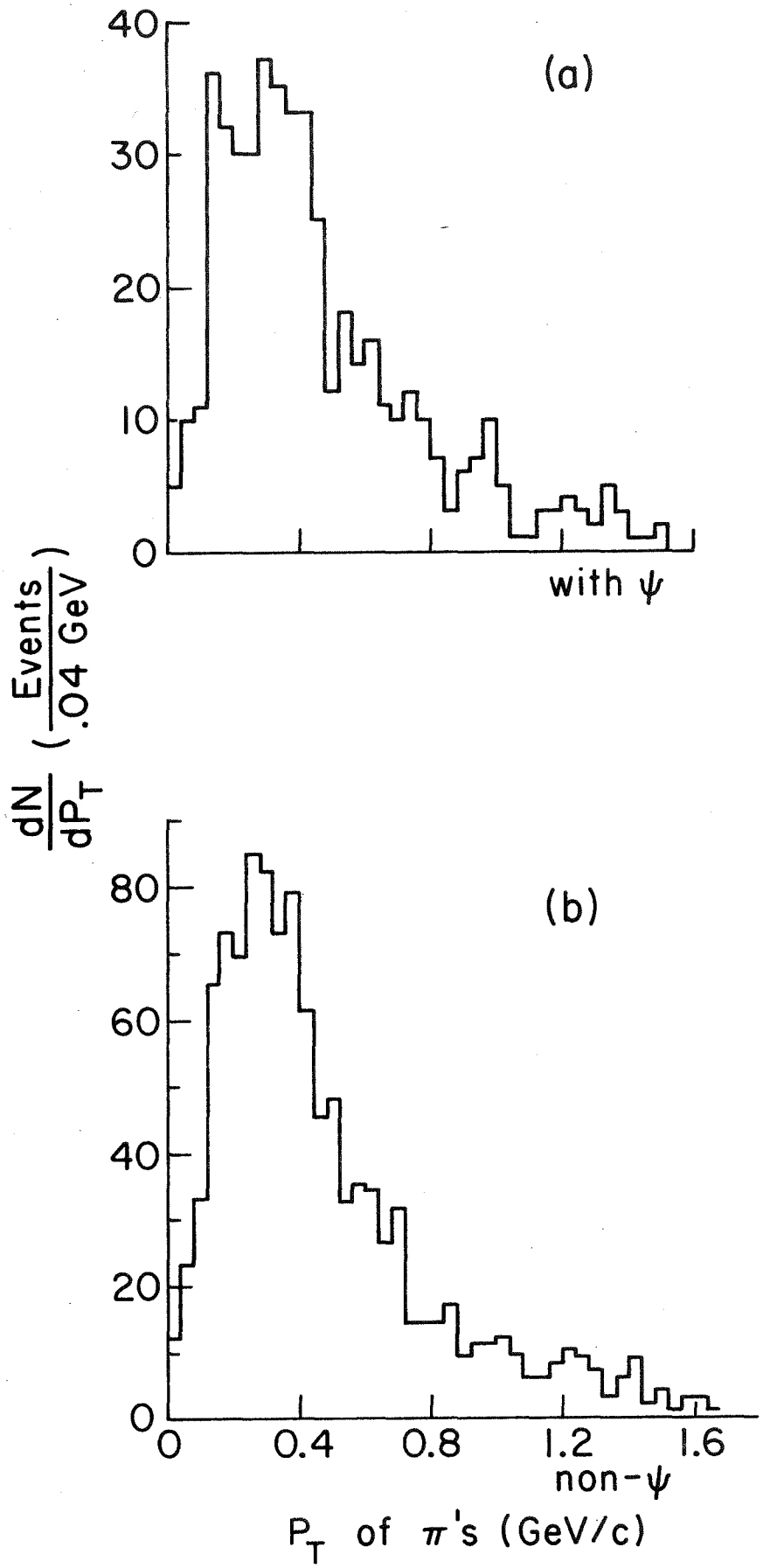
40
30
20
10
0
(a)
with ψ
dN/dP_T (Events/.04 GeV)
80
60
40
20
0
(b)
0
0.4
0.8
1.2
1.6
non-ψ
P_T of π's (GeV/c)

Figure 5-15.

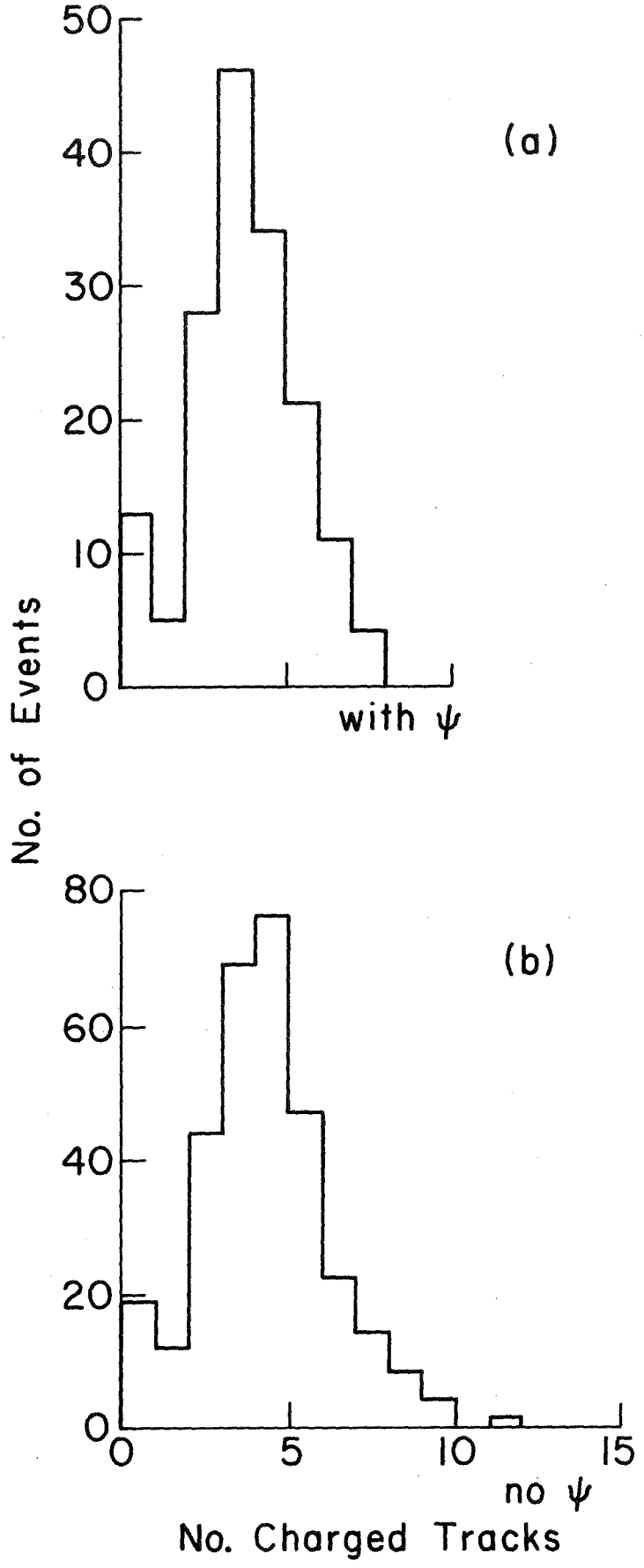
50
40
30
20
10
0
(a)
with ψ
No. of Events
80
60
40
20
0
(b)
0
5
10
15
no ψ
No. Charged Tracks

Figure 5-16.

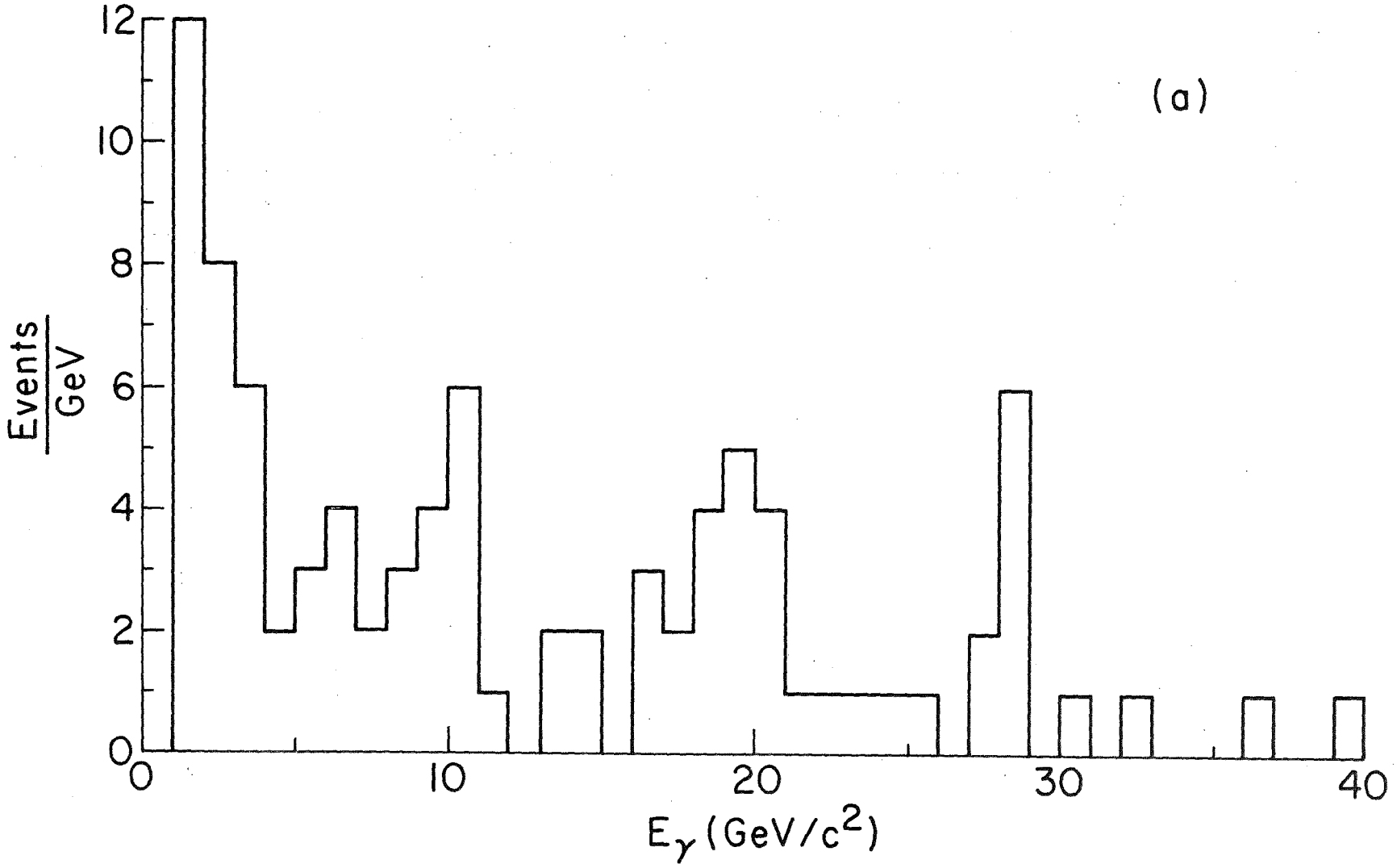

Figure 5-17. Energy of photons associated with ψ events.
(a) linear scale.

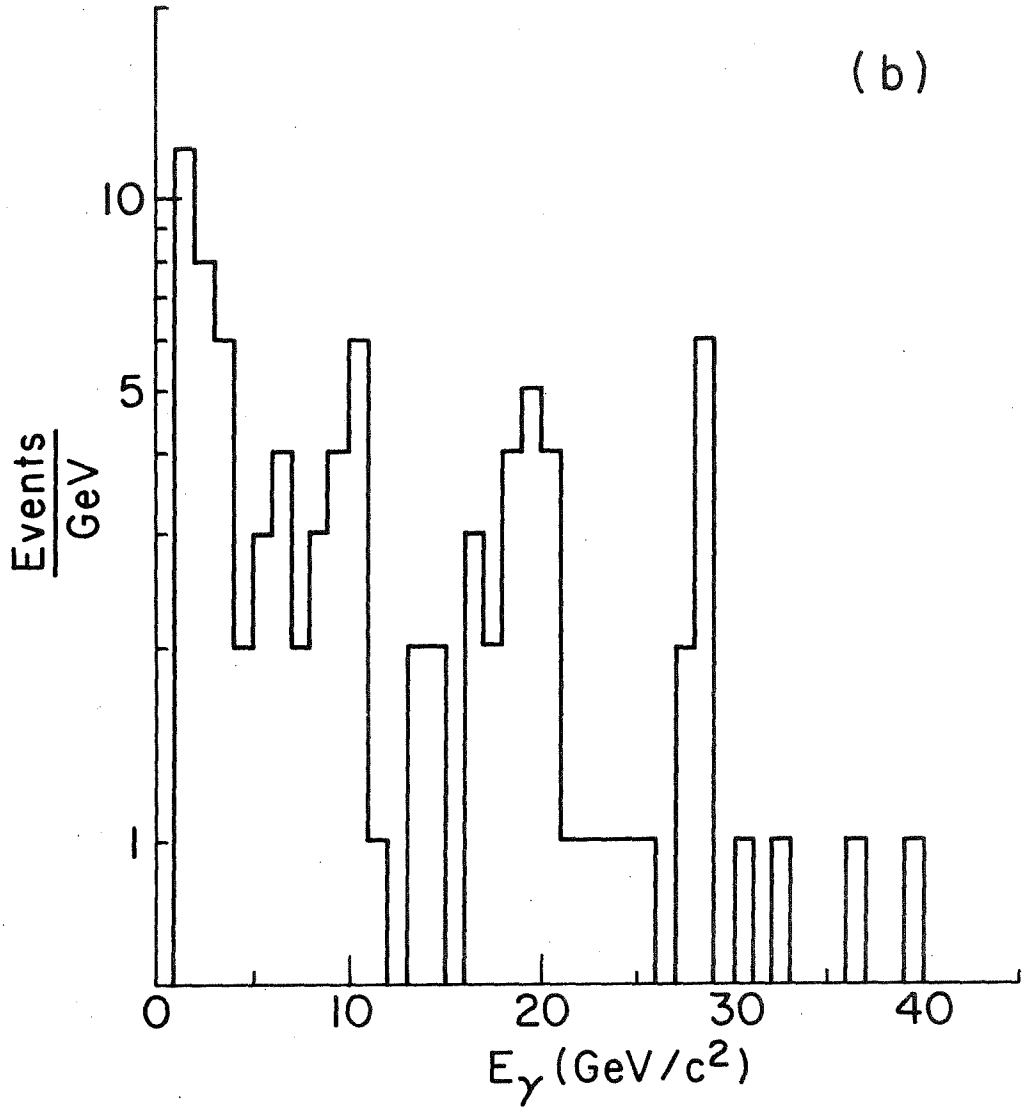

Figure 5-17. Energy of photons associated with ψ events. (b) semi-logarithmic scale.

We next have plotted the possible mass combinations created by adding psis and photons (Figure 5-18a) to make chi candidates. Each psi is combined in turn with all the photons found in the same event which pass all the cuts. Of the 92 mass combinations shown, 28 come from events with only one good photon. Those combinations using either of two photons with a diphoton mass compatible with a pi-zero were also removed.

Since we are mainly concerned with chis, in Figure 5-18b we have displayed the same mass spectrum with all combinations using a photon with a laboratory energy of less than 5 Gev deleted. Studies combining photons with various psis have shown that it would take a lab energy of around 10 Gev or greater to produce a psi-gamma mass combination in the region of the lowest lying chi, $\chi(3415)$. By removing these lower energy photons, we can tend to separate the problem of the low end of the spectrum from the chi region. This is made necessary because of the very low statistics involved in the region. With the full spectrum, the large number of events at the low end fool fitting routines because of the apparently low statistical error into matching the background and signal in this region. As there appears to be something anomalous going on at low mass, this would produce incorrect results.

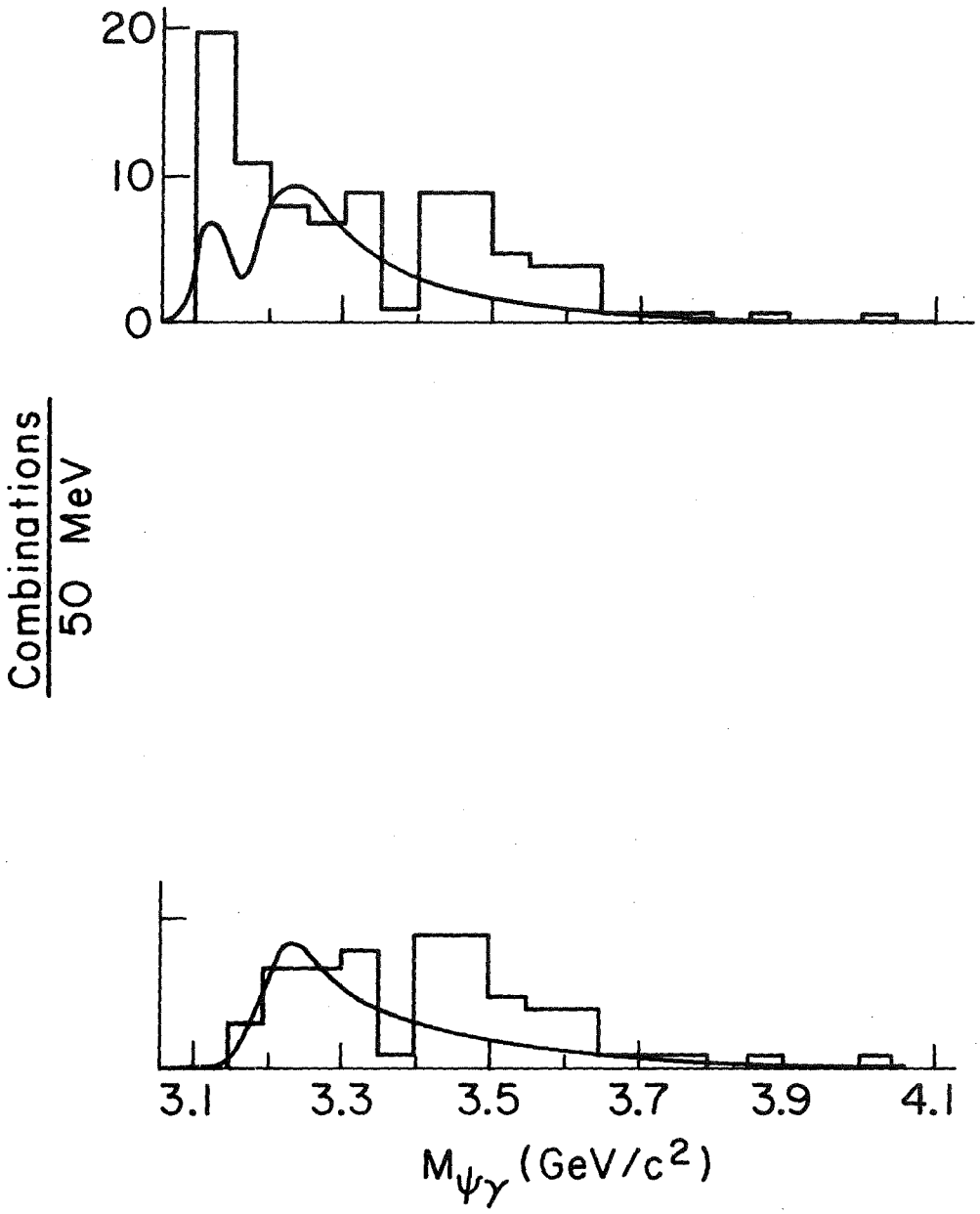

Figure 5-18. $\psi\gamma$ mass spectrum with background I superimposed.
(a) normal,
(b) with only E_γ > 5 GeV.

The resolution for psi-gamma mass combinations is poor enough that we cannot clearly isolate the signal from the background by inspection. As a result, a considerable study has been made of the various ways in which a background for these curves can be constructed. The smooth curves plotted against the solid histogram signal in Figures 5-18a and 5-18b were obtained by plotting the mass of the actual psis taken in combination with the photons from the dimuon events in the adjacent mass bins: 2.7-2.9 Gev and 3.3-4.0 Gev. By looking at the distributions from these regions separately, and also the region from 2.5-2.7 Gev, we have seen that there tends to be a mass dependence in backgrounds formed this way. To correct for this, we weight the distribution formed from combinations of the upper and lower mass regions so that each makes an equal contribution. To find the overall normalization for the background we divide the number of background combinations by the total number of background events. This method provides a total number of background events which, if the number of background and signal events were the same, is equal to the number of background photons. We took this as only a nominal value and let the normalization of the background shape be a floating parameter in the fitting procedure.

Using the same sort of procedure, we also tried combining psis with the photons from other psis. This produced a background with a shape much like that of the signal. If we removed those gammas and

psis which contributed to the chi region in the signal plot, a background plot was produced which was clearly biased the other way. This is due to the strong correlation between the energy of the photon and the psi-gamma mass. As a result, this procedure is not valid. Another method was to arbitrarily fix the mass of a non-psi dimuon event to that of the psi so we could form a background from non-psi dimuons with non-psi gammas. This shape was quite similar to that of psis combined with non-psi gammas but had the disadvantage of being one step further removed from what might be considered as the actual background.

A different way of approaching the background was to assume that all of the background photons came from the decay of pi-zeros. Since we have determined the distribution of charged pions, we can calculate the pi-zero spectrum using the assumption (see [8]) that the energy distribution for π° is the same as the distribution for $\frac{1}{2}(\pi^+ + \pi^-)$. It is then easy to get a photon spectrum, and thence a psi-gamma background spectrum. Lee Holloway has made this calculation using the data determined here at Illinois for the psi events. In Figure 5-19 we show the background from psis with non-psi gammas (dashed line, background I) and the background from the pion spectrum (solid line, background II). We note that in the chi region (3.35-3.6 Gev) the two backgrounds match quite well. There is a larger overall normalization error on the background from the pion spectrum as it requires a

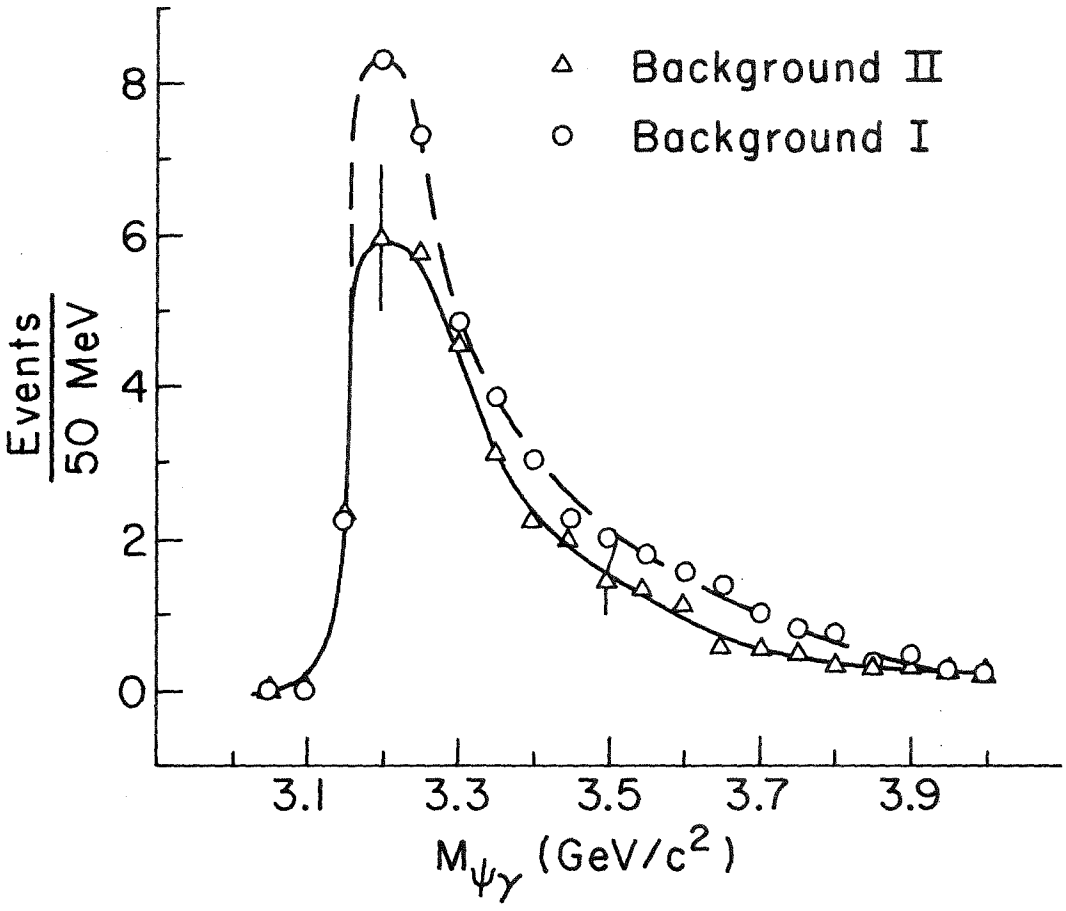

Figure 5-19. Background for $\psi\gamma$ spectrum.
I - gammas from non-psi events,
II - gammas derived from charged pion spectrum.

knowledge of the track-finding efficiency.

We have fit our psi-gamma spectrum and the various backgrounds to several hypotheses using the MINUIT fitting program as modified by U.E. Kruse. Given the particular background to be used, there were up to six parameters which could be allowed to float or to be clamped at a particular value. They were the amounts of background (COB) and either one or two resonanaces (COR1 and COR2), the masses of the resonances (M1 and M2), and the width of the resonances (S). The results of the various fits are presented in Table 5-2. The fixed values for M1 and M2 were the nominal values of 3.415 Gev and 3.550 Gev. The resonance width of 50 Mev is due to experimental resolution and is an estimate based on the reconstructed pi-zero width. A number quoted without error implies that the parameter was fixed at that value.

We would like to compare our results with the predictions of Carlson and Suaya discussed in Chapter 2. Their prediction for the production of the various chis was

$$\chi(3415):\chi(3510):\chi(3555) = 15:1:4 \quad . \tag{8}$$

We must modify this by a factor of (2j+1) where j is the spin of the chi to account for equal population of all spin states. When we fold in the measured branching ratio for the psi-gamma decay mode [9], we

then have the ratios 1:1.4:6.5. We neglect the $\chi(3510)$ as its production via two gluons is forbidden by the Landau-Pomeranchuk-Yang rule. This leaves us with the prediction that we should see $\chi(3415):\chi(3555)=1:6.5$. With the small number of events we have available, the uncertainty in the background , and our broad resolution, it would be difficult for us to say we confirm or disprove this prediction. Using the two resonance fit for comparison, however, it is certainly possible to say that we are consistent with this model. We note, however, that according to Brodsky and Gunion [10] as pointed out by Carlson and Suaya, if a $c\bar{c}$ pair is produced by gluon fusion, the average multiplicity of the event should be a factor of 9/4 higher than if it is produced by quark annihilation. Our multiplicity distributions are much the same both on and off the psi region (where reactions would not necessarily proceed through gluon fusion). This may not be significant, however, as our distribtions fail to include those charged particles (mostly those with an energy under 5 Gev) which fail to make it through the magnet. If the excess particles were concentrated at low x_F, they would not be counted in these distributions. Pi-zeros, however, can be detected at a somewhat lower x_F.

We have calculated the average multiplicity for charged pions and kaons for the same samples that were the basis for Figure 5-16. The average number of pions per event was 3.2 with a psi and 3.7 for a

non-psi events for kaons, the average was 1.2 and 1.1. In the 152 event psi sample, ther were 5 gamma-gamma mass combinations consistent with the pi-zero mass above a background of 4, while there were 3 pions above background for the dimuon events between 2.7-2.9 Gev and 3.3-4.0 Gev. All of these numbers have no efficiency or bias corrections.

The study of gamma rays produced in conjunction with psis has also been studied by two other groups at present: Cobb et. al. [11] and Clark et. al. [12]. (Yet another group, the Indiana-Saclay collaboration, is now adding a photon detector to their apparatus at CERN.) Cobb sees an excess of 25 +/- 9 events above background in the mass region $3.36 < m_{ee\gamma} < 3.72$ Gev. This leads to their figure

$$R = \left. \frac{B_{\chi\to\psi\gamma}\left(d\sigma_\chi/dy\right)}{\left(d\sigma_\psi/dy\right)} \right|_{y=o} = 0.43 \pm 0.21 \qquad (9)$$

at $\langle\sqrt{s}\rangle$ = 55 Gev, and where $B_{\chi\to\psi\gamma}$ is the branching ratio for the process $\chi\to\psi\gamma$. Clark, on the other hand, claims that they see no excess events in the range $400 < p_T < 600$ Mev/c, which is where the photon from chi decay would be with their experimental setup. They fit their distribution and find

$$R = 0.15 \begin{matrix} +0.1 \\ -0.15 \end{matrix} \qquad (10)$$

at $\sqrt{s}$= 52 and 63 Gev, which they feel is consistent with the gammas coming from pi-zero decay.

To try and make our own estimate of R, we fit the data with one resonance (see Table 5-2 again). Using our first background, we have 23 +/- 12 events attributable to chi production from our sample of 162 psis. This raw figure must be corrected for i) geometrical acceptance of gammas once a psi is detected--.19 +/- 0.01 (averaged over the 3.415 and 3.550 states), ii) the missing four blocks from our lead glass array-- 6% by area but only 4.1% by our Monte Carlo calculation, iii)the blocks lost in the beam region-- 0.8% by area or 1.8% by M.C., and iv) the quality cut. Referring back to Figures 4-5a and 4-5b we lost 2% of those electron showers with 75-100% of their energy in the center block of the shower and 19% of those showers with 50-75%. If we look at the number of pi-zeros reconstructed in Figure 4-6, however, we only have 50% reconstructed with our quality cut of $0<Q<10$. This would imply 29% losses for single showers. Using personal preference to pick the calibration tests as the more reliable, we claim to lose 15 +/- 5% because of the Q cut. This leads to an overall acceptance (where we use the Monte Carlo figures instead of geometrical figures, and the errors are due to the statistics on the Monte Carlo)

$$\text{Acceptance} = (0.19\pm0.01)(0.958\pm0.008)(0.982\pm0.005)(0.85\pm0.05) \quad (11)$$

$$= 0.15 \pm 0.012$$

Thus we have 153 +/- 81 chis after correction, or

$$\left.\frac{B_{\chi\to\psi\gamma}\sigma_{\chi}}{\sigma_{\psi}}\right|_{x_F\sim 0.5} = 0.94 \pm 0.50 \qquad (12)$$

which means that something like 50-100% of all psis are due to chi decay.

To close this discussion of the psi-gamma spectrum, we return to the signal before the E >5 Gev requirement was imposed. The reason this cut was originated was to remove the discrepancy between background and the signal in the region $3.1 < M_{\psi\gamma} < 3.2$ Gev. It is clear that there is something here that we don't understand. This excess of events could be an artifact of an incorrect background, or of something different between psi events and non-psi events. It may even be evidence for a new particle. This last possibility has been discussed recently in an internal memo [13] by R. Raja. He eliminates the possiblity that the excess is due to either i) the decay $\psi' \to \psi\pi^{\circ}\pi^{\circ}$ where the psions decay into photons, or ii) the decay of the charmonium state $^1D_2 \to \psi\omega$ (see also reference 14), where the decays to $\pi^+\pi^-\pi^{\circ}$ and thence produces two photons. A third very

interesting possible process discussed is due to the proposal by Lipkin [15] that the particle at 2.880 Gev is not the ^1S_o (η_c) state of charmonium, and that the real η_c should have a mass approximately that of the psi and a very large width (35 Mev). This would allow the decay $\eta_c \rightarrow \psi\gamma$ and produce a signal without a turnover as the mass approaches the psi, much as our signal appears.

There are several objections to this hypothesis, however. The transition rate between the and the psi should be proportional to $(m_{\eta_c} - m_\psi)^3$ and thus be very small. Finally, our estimate for R leasves very few psis that could be produced by anything except chi decay. This could be ignored if the acceptance for η_c production and decay were much higher than the one we calculated for chis, but this would require considerable kinematic juggling.

Interaction (Beam Momentum)	A	Confidence Level	B(GeV/c^{-1})	Confidence Level
$\pi^- p$ (217 GeV/c)	1.13 ± 0.31	0.15	1.69 ± 0.23	0.90
$\pi^- Be$	1.12 ± 0.29	0.20	1.50 ± 0.23	0.59
$\pi^- Fe$[a] (200 GeV/c)	1.20 ± 0.20	----	1.60 ± 0.20	----
$\pi^- C$[b] (225 GeV/c)	1.93 ± 0.20	----	1.98 ± 0.13	----
$\pi^+ C$[b]	1.33 ± 0.21	----	2.06 ± 0.10	----

[a] These results are from Reference 5.

[b] These results are from Reference 6.

Table 5-1.

Psi Fit Parameters.
Invariant cross section after acceptance corrections is fitted in the region 0.1-0.9 for x_F and 0.0-3.2 GeV/c for p_T.

COR 1	COR 2	COB	M1	M2	SDEV	χ^2	^{o}freedom	CONLEV
18.4 ± 15.8	11.1 ± 7.3	0.84 ± 0.37	3.410	3.550	0.120 ± 0.09	8.39	15	0.91
15.8 ± 11.2	12.6 ± 7.2	1.10 ± 0.37	3.410	3.550	0.120 ± 0.06	7.62	15	0.94
12.6 ± 6.2	9.5 ± 5.3	1.04 ± 0.23	3.410	3.550	0.060	11.09	16	0.80
11.9 ± 5.9	9.9 ± 5.3	1.33 ± 0.29	3.410	3.550	0.060	10.05	16	0.86
		1.68 ± 0.22				21.23	18	0.27
		2.13 ± 0.29				20.29	18	0.32
23.3 ± 11.8		0.98 ± 0.31	3.48 ± 0.04		0.12 ± 0.06	7.80	15	0.93
23.4 ± 9.9		1.25 ± 0.34	3.49 ± 0.03		0.12 ± 0.05	6.95	15	0.96

Table 5-2.
Fits to $M_{\psi\gamma}$. Each fit is performed using Background I and Background II.

Chapter 5 References

1. J.G. Branson et al., Phys. Rev. Lett. 38, 1331 (1977).

2. Particle Data Group, Rev. Mod. Phys. 48, (1976).

3. B.L. Ioffe, Phys. Rev. Lett. 39, 1589 (1977).

4. K.V. Vasavada, Phys. Rev. D16, 146 (1977).

5. G.J. Blanar et al., Phys. Rev. Lett. 35, 346 (1975)
M.L. Mallary et al., Proceedings of the 1976 Vanderbilt Conference, ed. by R.S. Panvini, AIP Conf. Proc. No. 30, page 94 (1976).

6. J.G. Branson et al., Phys. Rev. Lett. 38, 1334 (1977).

7. M. Binkley et al., Phys. Rev. Lett. 37, 571 (1976).

8. J. Whitmore et al., Phys. Rep. 10C, 273 (1974).

9. Particle Data Group, Phys. Lett. 75B, 1 (1978).

10. S. Brodsky and J. Gunion, Phys. Rev. Lett. 37, 402 (1976).

11. J.H. Cobb et al., Phys. Lett. 72B, 497 (1978).

12. A.G. Clark et al., Nuc. Phys. B142, 29 (1978).

13. R. Raja, unpublished communication to E369 collaborators, Dec. 1978.

14. Fermilab proposal P610.

15. H.J. Lipkin, H.R. Rubinstein, and N. Isgur, Wisconsin preprint,WIS-78/23 Ph.

16. W. Bartel et al., Phys. Lett. 79B, 492 (1978).

VITA

George Oscar Alverson [redacted]. He received the Bachelor of Science degree in Physics and English from the California Institute of Technology in 1973, and a Master of Science degree from the University of Illinois in 1974. He was a University Fellow during 1973-1974, and worked as a teaching assistant and as a research assistant.